



One kilometre-thick ultramylonite, Sierra de Quilmes, Sierras Pampeanas, NW Argentina



M.A. Finch ^{a,*}, R.F. Weinberg ^a, M.G. Fuentes ^b, P. Hasalová ^{a,c}, R. Becchio ^b

^a School of Earth, Atmosphere and Environment, Monash University, Clayton, VIC 3800, Australia

^b Instituto Geonorte, National University of Salta, INENCO-CONICET, Av. Bolivia 5150, 4400 Salta, Argentina

^c Centre for Lithospheric Research, Czech Geological Survey, Klárov 3, 118 21 Prague 1, Czech Republic

ARTICLE INFO

Article history:

Received 15 September 2014

Received in revised form

17 December 2014

Accepted 4 January 2015

Available online 13 January 2015

Keywords:

Ultramylonite

Sierra de Quilmes

Sierras Pampeanas

Famatinian orogeny

Shear zone width

ABSTRACT

We describe a 1 km-thick ultramylonite forming the high strain base of the >3.5 km-thick El Pichao shear zone in the Sierra de Quilmes. This shear zone thrusts granulite facies migmatites onto amphibolite facies rocks during the 470 Ma Famatinian orogeny. Strain grades upwards from ultramylonites to weakly sheared migmatites across the 3.5 km-zone and the mylonitic rocks define a geochemical field narrower than the protolith, suggesting they underwent mixing and homogenization through shearing. Ultramylonites this thick are uncommon. The width of a shear zone, in the absence of significant compositional rheological contrasts controlling strain localization, is controlled by the balance between shear heat generation and diffusion. Under typical crustal conditions a strain rate of 10^{-12} s^{-1} is required to form a 1 km-thick ultramylonite, and this is achieved when large movement velocities are imposed across the shear zone. We postulate that the El Pichao shear zone and its thick ultramylonite accommodated a significant fraction of convergence velocities driving the orogeny, and that the wide mylonitic shear zones characteristic of the Cambrian–Ordovician deformation of the Sierras Pampeanas result from the convergent movement being taken up by only a few active major shear zones.

© 2015 Elsevier Ltd. All rights reserved.

1. Introduction

Mylonitic shear zones are localized zones of high strain developed during ductile deformation. Shear zones nucleate at sites of (i) pre-existing heterogeneities, either compositional (e.g. layering) or mechanical (faults, cracks, joints; inherited localization model; e.g. Pennacchioni and Mancktelow, 2007), (ii) weak, anastomosing micro-shear instabilities (widening model; e.g. Ingles et al., 1999), (iii) strain softening caused by grain size reduction and change of active deformation mechanisms and/or fluid ingress (dynamic localization model; Montési and Zuber, 2002; Jessell et al., 2005; Oliot et al., 2010), and (iv) higher shear heating (Regenauer-Lieb and Yuen, 1998; Regenauer-Lieb et al., 2006). After nucleation, mylonitic shear zones may thicken if the shear zone hardens and it becomes easier to deform its margins (type 1 of Means, 1995). Shear zones may also weaken further (type 2) due to strain softening (e.g. White et al., 1980; Fliervoet et al., 1997; Kilian et al., 2011) which is a result of the development of crystallographic preferred orientation

(White et al., 1980; Ji et al., 2004), reaction softening (e.g. Hippertt and Hongn, 1998; Jefferies et al., 2006; Oliot et al., 2010; Goncalves et al., 2012), and shear heating (Regenauer-Lieb et al., 2006). Weakening processes are related to fluid ingress into the shear zone which facilitates the retrogression of minerals and enhances recrystallization mechanisms (e.g. White et al., 1980; Stunitz and Gerald, 1993; Hippertt, 1998; O'Hara, 2007), particularly dissolution–precipitation (e.g. Sinha et al., 1986; Jefferies et al., 2006; O'Hara, 2007) and diffusive mass transfer (Hippertt, 1998; Hippertt and Hongn, 1998; Jefferies et al., 2006).

Shear zones are usually narrow relative to the width of the deforming region due to strain localization. It has been argued that shear zone width relates to the combination of yield stress (a function of temperature and depth), plate velocity, and strain rate, which increases as the shear zone weakens at constant stress (Platt and Behr, 2011). However, Vauchez et al. (2012) determined that these variables are not independent because strain rate determines the yield stress of rock and strain rate itself depends on the width of the shear zone. Instead, they proposed that the thickness of the shear zone is optimised to minimise work (strain rate times stress). Shear zones are narrow in the upper crust where rocks are strong, and widen with depth as temperature increases and rocks become

* Corresponding author.

E-mail address: melanie.finch@monash.edu (M.A. Finch).

weaker. Indeed, it has been shown that in the middle to lower crust shear zones can be tens of kilometres wide with a concomitant decrease in strain intensity (Vauchez and Tommasi, 2003; Vauchez et al., 2007).

In a homogeneous rock mass, shear zone width depends on the balance between shear heating (a function of strain rate) and heat diffusion away from the fault, modulated by the sensitivity of rock viscosity to temperature (Regenauer-Lieb and Yuen, 1998). Both the strain rate and the stress distribution in shear zones can be variable through time and space due to the contemporaneous evolution of a set of shear zones that together accommodate lithospheric straining, as well as to the role of storage and release of elastic energy (Regenauer-Lieb et al., 2006, 2012). Regenauer-Lieb et al. (2012), investigating the strength of the lithosphere showed how it weakens considerably as a network of shear zones develops to accommodate deformation. They showed that the spatial distribution and width of shear zones, as well as how effectively deformation is localized into them, depend on whether the lithosphere was initially hot or cold. Shear zone networks in hot, weak lithospheres are wider and less efficient at weakening the lithosphere when compared to networks in colder lithospheres. The net effect is that the strength of hot and cold lithospheres tends to converge as the shear zone network matures.

In hot but sub-solidus conditions, mylonites develop readily because of the lack of rheological bimodality between feldspar and quartz (e.g. Tullis and Yund, 1985; Hanmer et al., 1995) so that both minerals recrystallize without development of feldspar porphyroclasts (Hanmer et al., 1995). Cases such as these may be identified by the absence of strain gradient at the margins of the mylonitic zone (Hanmer et al., 1995). In contrast, lower temperature ultramylonites formed at greenschist or amphibolite facies are a result of strong strain localization and most commonly occur as cm-sized bands within mylonitic and protomylonitic shear zones (Whitmeyer and Simpson, 2003).

Shear zones commonly show a strain gradient from low strain protomylonites at the edge, to high strain ultramylonites in the centre of the shear zone (e.g. Kilian et al., 2011). The degree of mylonitization is indicated by a progressive increase in the proportion of recrystallized matrix relative to porphyroclasts (Sibson, 1977). Ultramylonites, defined as rocks where more than 90% of the crystals are recrystallized (Sibson, 1977), are the ultimate product of mylonitization. Ultramylonites can be relatively coarse-grained at high temperatures, and grain size decreases to very fine at greenschist facies (Trouw et al., 2010). Ultramylonitic shear zones are commonly fluid conduits and show mass loss or gain in comparison to adjacent protomylonites and mylonites (e.g. Hippertt, 1998; Hippertt and Hongn, 1998; Jefferies et al., 2006). They are commonly enriched in phyllosilicates (mica and chlorite at low temperatures) due to mineral hydration (Hippertt and Hongn, 1998; O'Hara, 2007) and any porphyroclasts that remain are rounded from shear-induced erosion and recrystallization during rotation (e.g. Hippertt and Hongn, 1998; Griera et al., 2011). In contrast to protomylonites and mylonites, many ultramylonites contain few quartz ribbons and lack compositional layering due to homogenization of the matrix and mixing of the different phases (e.g. Fliervoet et al., 1997; Kanagawa et al., 2008; Kilian et al., 2011). This is a result of grain boundary sliding accommodated by diffusion creep (e.g. Tullis et al., 1982; Garlick and Gromet, 2004) accompanied in some cases by dissolution–precipitation (Kilian et al., 2011). Although rarer, layered ultramylonites can develop if there is high ductility contrast between layers which causes strain to partition into the weakest layer (Ishii et al., 2007). Ultramylonites at amphibolite to greenschist facies commonly have a fine-grained, dark-grey to green or black matrix and consist dominantly of quartz, feldspar, and biotite with fewer than 10% feldspar

porphyroclasts (e.g. Sinha et al., 1986; Jefferies et al., 2006; Ishii et al., 2007). Ultramylonites are usually synonymous with high strain. However, because they are defined by recrystallization of grains generally accompanied by the loss of porphyroclasts, they can form at lower strains when the protolith is fine-grained with few porphyroclasts (Trouw et al., 2010) or when deformation is at high temperatures and feldspar porphyroclasts become as ductile as quartz (e.g. Tullis and Yund, 1985; Hammer et al., 1995).

Thick ultramylonitic shear zones are rare in the Earth's crust because in the upper crust strain typically localises to thin bands, whereas in the lower crust, strain is distributed over a wide area of lower strain. Despite these expectations, thick sequences of ultramylonites are occasionally reported. Ultramylonites 300–400 m thick are found in the shear zones related to the Pan-African orogeny and amalgamation of West Gondwana in NW Africa (Ferkous and Leblanc, 1995; Arthaud et al., 2008). Similarly, the Mulgandinnah shear zone in Western Australia contains a 500 m-thick zone of ultramylonite which formed in response to accretion and formation of the Pilbara terrane (Zegers et al., 1998). The Corredoiras detachment in NW Spain also contains a 500 m-wide section of ultramylonite and mylonite which accommodated at least 10 km of thrusting during Variscan plate convergence (Díaz García et al., 1999). Where they occur, thick ultramylonites are related to major tectonic boundaries. This paper describes the nature of a very thick ultramylonite of the El Pichao shear zone in the Sierra de Quilmes, part of the Sierras Pampeanas mountain range in NW Argentina.

In this paper we follow Sibson's (1977) classification, with protomylonites consisting <50% recrystallized matrix, mylonites consisting of between 50 and 90% recrystallized matrix, and ultramylonites consisting of >90% recrystallized matrix. We use 'mylonitic rocks' as a collective term referring to rocks ranging from ultramylonites to protomylonites and the term 'mylonite' according to Sibson's definition.

2. Geological setting of the Sierra de Quilmes

The Sierras Pampeanas were exhumed in the foreland of the Andean orogen (Fig. 1; Jordan and Allmendinger, 1986; Rapela et al., 1998a) and dominantly consist of metamorphosed rocks of the Puncoviscana formation (Turner, 1960). This formation is a turbidite sequence that consists of sediments eroded from the southwest Gondwana craton (Acenolaza et al., 1988; Schwartz and Gromet, 2004) and deposited on the palaeo-Pacific margin of Gondwana (e.g. Jezek et al., 1985). It was deposited between 600 and 530 Ma (Rapela et al., 1998b; Sims et al., 1998; Schwartz and Gromet, 2004), although the maximum age is unknown because the base of the formation is nowhere seen (Jezek et al., 1985). It outcrops over an area of 1200 km × 300 km from south Bolivia to central Argentina (Fig. 1a; Jezek et al., 1985).

During the Palaeozoic the Puncoviscana formation was metamorphosed and deformed during at least two overlapping tectono-thermal episodes on the paleo-Pacific margin of Gondwana (Acenolaza et al., 1988). The first event was in the Early to Middle Cambrian (535–515 Ma) and caused the Pampean orogeny which resulted in the formation of a magmatic arc and granulite facies metamorphism and anatexis (Rapela et al., 1998a,b). The second event was in the Ordovician (490–450 Ma) and caused the Famatinian orogeny which resulted in continental arc magmatism (Rapela et al., 1998a; Sims et al., 1998) and the development of a back-arc basin (Rapela et al., 1998a). The Oclroyic tectonic phase (450–430 Ma; Bahlburg and Herve, 1997; Rapela et al., 1998a) caused shortening and closure of the Famatinian back-arc basin (Dalla Salda et al., 1992; Rapela et al., 1998a; Astini and Davila, 2004; Castro de Machuca et al., 2012). In the northern Sierras

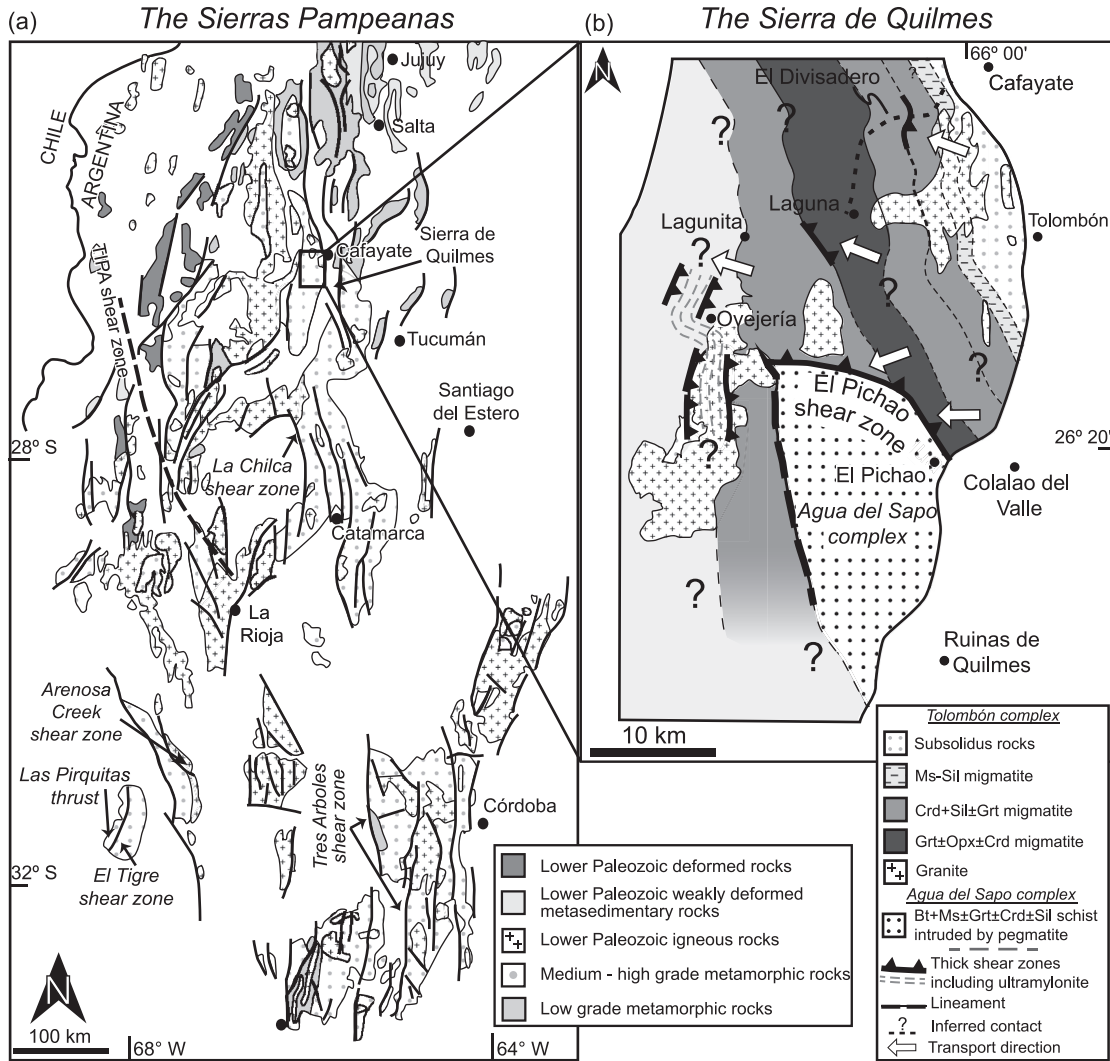


Fig. 1. The Sierras Pampeanas and Sierra de Quilmes of NW Argentina. (a) The Sierras Pampeanas with the location of major faults and shear zones indicated (modified from [Hongn et al., 2010](#)). The area shown in (b) is boxed. (b) The studied area in Sierra de Quilmes with El Pichao shear zone indicated in east of range. Granitic bodies are ultramylonitic close to thrusts.

Pampeanas, the absence of exotic terranes, mafic magmatism, and high pressure metamorphism (e.g. [Lucassen et al., 2000, 2011](#)) indicate a high-temperature, low-pressure regime between 535 and 430 Ma during consecutive Pampean and Famatinian orogenies ([Lucassen et al., 2000, 2011](#)). There is no evidence to support models which propose continental collision and crustal thickening processes ([Ramos, 1988](#) and references therein, [Omarini et al., 1999](#), [Loewy et al., 2004](#)) in the northern Sierras Pampeanas.

Shear zones resulting from these orogenies are common in the Sierras Pampeanas and occur discontinuously over 1000 km from 33° S to at least 24° S, and spread over a width of >250 km ([Fig. 1a](#); [Höckenreiner et al., 2003](#)). These shear zones are commonly thick zones of mylonite and ultramylonite with thrust-to-west shear sense ([Fig. 1](#); e.g. [Le Corre and Rossello, 1994](#); [Whitmeyer and Simpson, 2003](#); [Lopez et al., 2007](#); [Larrovere et al., 2008](#); [Castro de Machuca et al., 2010](#); [Castro de Machuca et al., 2012](#)). One of the most significant shear zones in the northern Sierras Pampeanas is the Tinogasta–Pituiñ–Antinaco (TIPA) shear zone ([Lopez and Toselli, 1993](#)) part of the Las Termas belt in NW Argentina ([Fig. 1a](#)). The TIPA shear zone is ~2 km thick, 300 km long and contains mylonites that are increasingly deformed toward the centre of the zone ([Höckenreiner et al., 2003](#)). The TIPA shear zone was active at ~400 Ma and thrusts Precambrian–Cambrian rocks west onto

granitoids of the Famatinian magmatic arc ([Höckenreiner et al., 2003](#)). It is the largest of several shear zones that trend NNW–SSE in the region between La Rioja and Sierra de Quilmes ([Fig. 1a](#)). Clusters of shear zones are also seen in the southern Sierras Pampeanas in Sierras de Córdoba where [Martino \(2003\)](#) recognised 16 shear zones that accommodated thrusting and of these the Tres Arboles shear zone is the most significant at a length of 150 km and width of up to 16 km ([Fig. 1a](#); [Whitmeyer and Simpson, 2003](#)). Like the shear zones in the north, the Tres Arboles shear zone trends NNW and thrusts Cambrian schists onto Ordovician rocks ([Whitmeyer and Simpson, 2003](#)). Northwest of Sierras de Córdoba, the Sierra de Velasco contains six shear zones which trend NNW. One of the largest is La Horqueta shear zone, which is up to 2 km thick and contains protomylonites and mylonites with a sinistral-thrust shear sense ([Lopez et al., 2007](#)). Ductile shear zones have also been recognized in southern Puna and the Eastern Cordillera and overprint igneous and metamorphic rocks ([Hongn et al., 1996](#); [Lucassen and Becchio, 2003](#)) including the Brealito shear zone ([Hongn and Becchio, 1999](#)), the Agua Rosada shear zone ([Hongn and Riller, 2007](#)), and shear zones in Sierra de Molinos ([Sola et al., 2010](#)). Combined, these and other shear zones cropping out in the Sierras Pampeanas accommodated major periods of convergence on the paleo-Pacific margin of Gondwana.

The Sierra de Quilmes is a 140 km long N–S trending mountain in the northern Sierras Pampeanas west of the town of Cafayate (Fig. 1; Rossi De Toselli et al., 1976). It consists of two metamorphic complexes: the granulite facies Tolombón complex to the north and west of the range, and the amphibolite facies Agua del Sapo complex in the east and south of the range (Fig. 1b; Toselli et al., 1978). On the east side of the Sierra de Quilmes, the Tolombón complex is thrust onto the Agua del Sapo complex along a NW–SE trending shear zone: the El Pichao shear zone described in this paper. In the centre of Sierra de Quilmes, the western margin of the Agua del Sapo complex is also in fault contact with the Tolombón complex forming an NNW–SSE-trending sub-vertical greenschist facies ultramylonitic shear zone that defines a long lineament (Fig. 1b). Both

complexes consist of metamorphosed sedimentary rocks of the Puncoviscana formation that were located in the upper to middle crust during metamorphism and underlie the lower grade rocks exposed in other mountains of the Sierras Pampeanas to the north (Toselli et al., 1978; Becchio et al., 1999; Büttner et al., 2005). The Agua del Sapo complex consists of gneisses and metasedimentary rocks containing $Qtz+Pl+Bt+Ms+Ksp\pm Grt\pm Tur\pm Hbl\pm Crd\pm Ep$ (mineral abbreviations after Whitney and Evans, 2010) intruded by Grt-pegmatite dykes (Toselli et al., 1978). Grt-schists are common in the north of the complex, and occasionally contain cordierite. Nodules up to 2 m in length and discontinuous layers of calc-silicate are common.

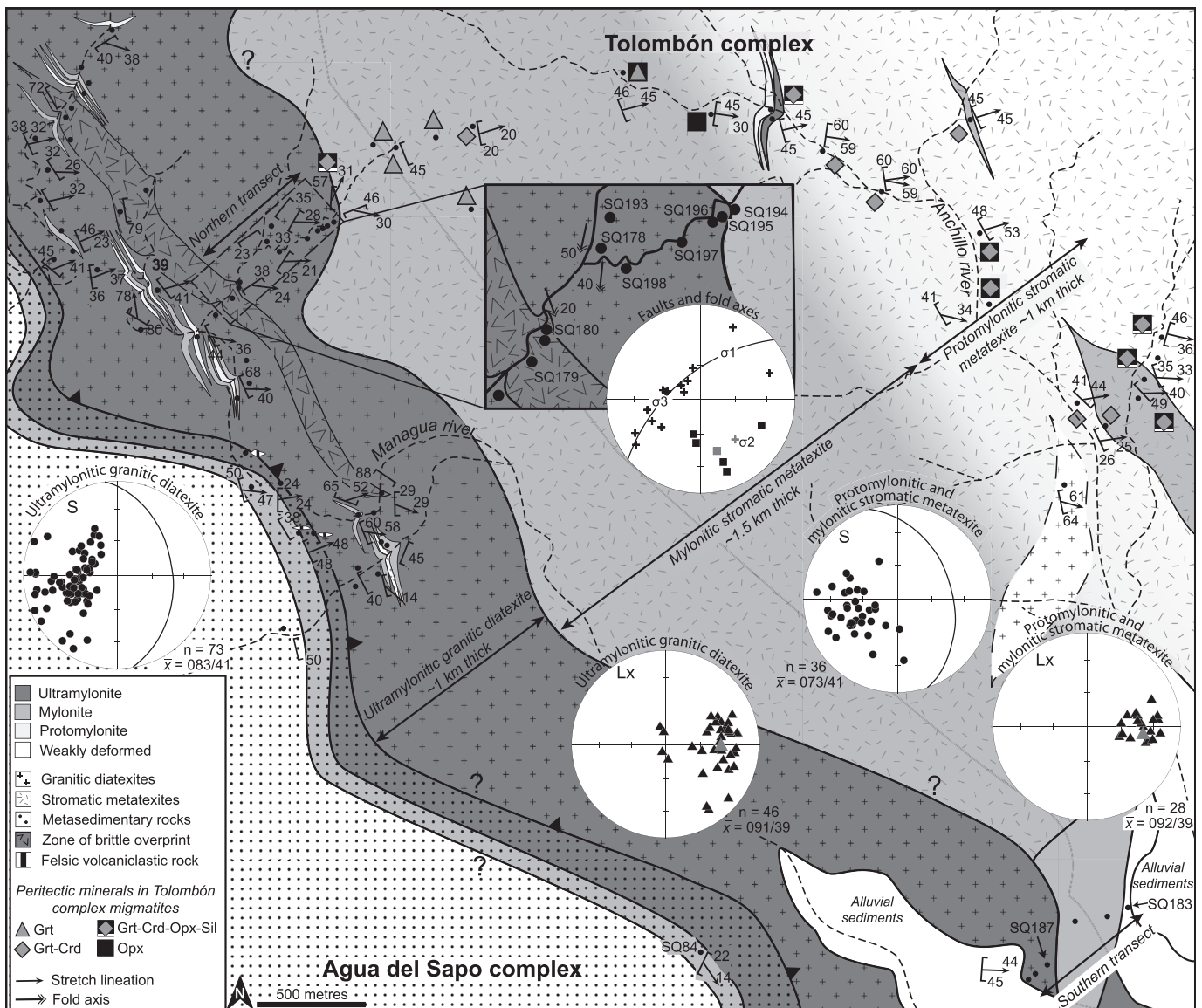


Fig. 2. Geological map of El Pichao shear zone showing thrusting of granulite facies migmatites of the Tolombón complex onto amphibolite facies meta-psammmites and -pelites of the Agua del Sapo complex. Mapping mostly followed river gorges due to limited access to mountain ridges, waypoints are marked by black circles. The main shear plane dips NE with a down-dip stretching lineation (stereonet). All stereographic projections are lower hemisphere equal-area, the mean plane (\bar{x}) indicated with a great circle and mean lineation with a grey triangle. The stereographic projection for the ultramylonitic diatexite layer shows a spread of foliation measurements from NE to SE dipping. The intersection of these planes is parallel to the stretching lineation and defines the axis of open folds or undulations of thrust planes. Map inset: zoom-in of the northern transect with stereographic projection of poles to fault planes (black crosses) defining great circle, fold axes (black squares), and mean fold axis (grey square). σ_2 is the intersection of all fault planes (pole to great circle, grey cross). σ_1 and σ_3 are on the great circle but remain ill-defined because of lack of striations on the fault planes. σ_1 is inferred to plunge east because of thrusting sense documented in a few of these NE through to SE dipping fault planes.

The Tolombón complex consists of interbedded psammities and pelites, including calc-silicate pods and layers, that grade from greenschist facies in the northeast of the Sierra de Quilmes, to granulite facies migmatites in the southwest, indicating a tilted metamorphic sequence (Fig. 2). Anatexis is linked to the presence of diatexite–granite bodies including the composite Cafayate pluton near El Divisadero (Fig. 2). Büttner et al. (2005) divided the Tolombón complex in the region of El Divisadero, west of Cafayate town, into four metamorphic zones: from northeast to southwest these are the low grade chlorite zone that grades into the biotite–muscovite zone, followed by the garnet–cordierite–sillimanite zone, and finally the highest grade orthopyroxene zone. Ms-dehydration melting begins in the biotite–muscovite zone and continues into the garnet–cordierite–sillimanite zone where it is accompanied by Bt-dehydration melting (Büttner et al., 2005). The orthopyroxene zone contains migmatites produced through Bt-dehydration melting with leucosomes that contain $\text{Opx} + \text{Grt} \pm \text{Crd} \pm \text{Ksp}$ (Büttner et al., 2005). Metamorphism was high-temperature and low-to medium-pressure (500–800 °C, 3.5–6 kbar; Rapela, 1976; Toselli et al., 1978; Büttner et al., 2005) and peak metamorphism occurred at ~470 Ma (U–Pb monazite and titanite, ICP–MS; Büttner et al., 2005) as part of the Famatinian orogeny. Anatexis and peak metamorphism were coeval with ductile thrusting verging to the west, which ended by ~440 Ma (Büttner et al., 2005). Büttner (2009) suggested that shear zones were originally horizontal and extensional, and later rotated by Andean uplift to show apparent thrust shear sense. This interpretation is not consistent with our findings and will be discussed later.

3. The El Pichao shear zone (PSZ)

The shear zone was named after El Pichao village in its proximity. It thrusts the Grt–Crd–Opx migmatites of the Tolombón complex onto the Grt-bearing metasedimentary rocks of the Agua del Sapo complex (Toselli et al., 1978; Figs. 1 and 2). Above and NE of the shear zone, the Tolombón complex consists of weakly deformed stromatic metatexites and diatexites (described in Section 3.1). These rocks grade to the SW into a 1 km-thick layer of protomylonitic stromatic metatexite (Section 3.2), followed by a 1.5 km-thick layer of mylonitic stromatic metatexite (Section 3.3), and at the base of the shear zone, a 1 km-thick layer of ultramylonitic granitic diatexite (Section 3.4). For simplicity these layers are referred to as protomylonitic metatexite, mylonitic metatexite, and ultramylonitic diatexite respectively. Below the ultramylonitic diatexite there is a sharp contact with the ultramylonitic top of the Agua del Sapo complex that grades downwards into interbedded meta-psammite and -pelite (Section 3.5). The El Pichao shear zone is ~3.5 km thick and comprises the protomylonitic and mylonitic metatexite, the ultramylonitic diatexite and the mylonitic top of the

Agua del Sapo complex. The rocks in each section and transitions between them are described below.

3.1. Tolombón complex: weakly deformed migmatites of the hanging wall

Northeast of and structurally above the PSZ, the Tolombón complex consists of weakly deformed migmatites characterized by leucosomes and melanosomes and evidence for magma flow and extraction (migmatite terminology after Mehnert, 1968). Leucosomes are thick, continuous leucocratic bands which contain peritectic minerals (Grt, Opx, Crd; Fig. 4a), coarse flakes of biotite rimming peritectic minerals (Fig. 4b) interpreted to result from reaction with melt during crystallization, symplectitic garnet–quartz intergrowths (Fig. 4c), and leucosomes which intrude across melanosome layers (Fig. 4a) or are aligned with S–C planes or axial planes of folds (Fig. 4d,e). These features are interpreted to be primary and a result of anatexis with little subsequent modification.

Migmatites are typically stromatic metatexites (Fig. 4a) that grade into regions of diatexite (where the rock loses coherency and behaves as a magma, neosome > paleosome) and granitic diatexite (neosome > 90%). Stromatic migmatites contain >20% leucosome (Fig. 4a) and peritectic minerals appear in both leucosome and melanosome. They also show compositional banding with layers of sand-sized grains of quartz, feldspar, biotite, and garnet that alternate with layers of finer grain size that contain mica, feldspar, quartz, and garnet. This is interpreted as bedding from the protolith which forms well-foliated, leucosome-rich pelitic layers (~80% of total outcrop) and weakly-foliated, leucosome-poor psammitic layers (~20%; Fig. 4a). Leucosomes contain peritectic garnet, cordierite, and orthopyroxene in different combinations and modal proportions: garnet is common to both the psammitic and pelitic rocks but orthopyroxene is more common in psammite, and cordierite in pelite (Fig. 4a,c). Garnet is also found in melanosomes and it is almost always present in metatexites with the exception of a small number of Opx-bearing psammitic layers. Cordierite also appears in melanosomes (Fig. 4c) and occurs only in combination with garnet and/or orthopyroxene. Diatexites are essentially the same as metatexites but due to the higher melt fraction they have lost coherence and layering is disaggregated into a chaotic mass of magma and schollen. Granitic diatexites are porphyritic and contain small (<30 cm long) schollen of meta-psammite and -pelite.

The contact between weakly deformed migmatites and the mylonitic rocks of the PSZ is gradual and marked by an increase in the intensity of foliation towards the SW as rocks become gneissic then protomylonitic (Fig. 5a). The boundary defining the top of the PSZ is placed NE of Anchillo river gorge (Fig. 2) where the

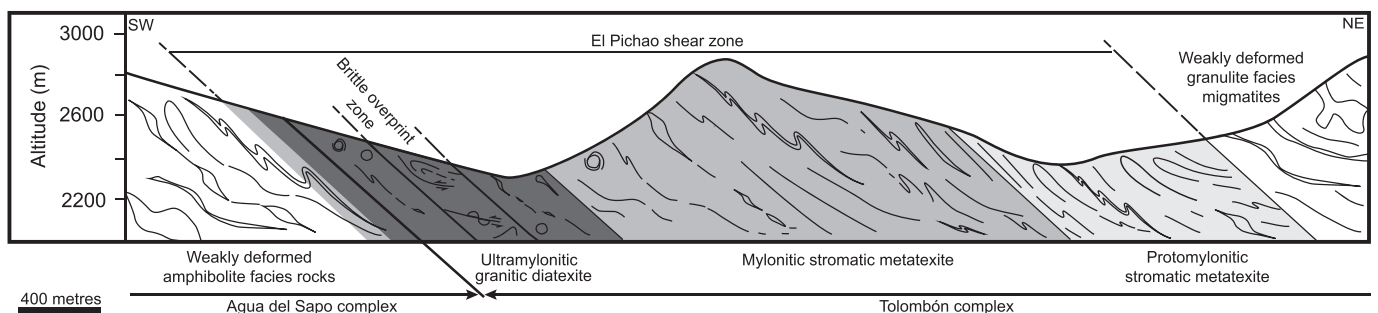


Fig. 3. Schematic cross section showing the layers of the El Pichao shear zone discussed in the main text. Contacts between layers are transitional over 10–20 m and dips of contacts and structures are means.

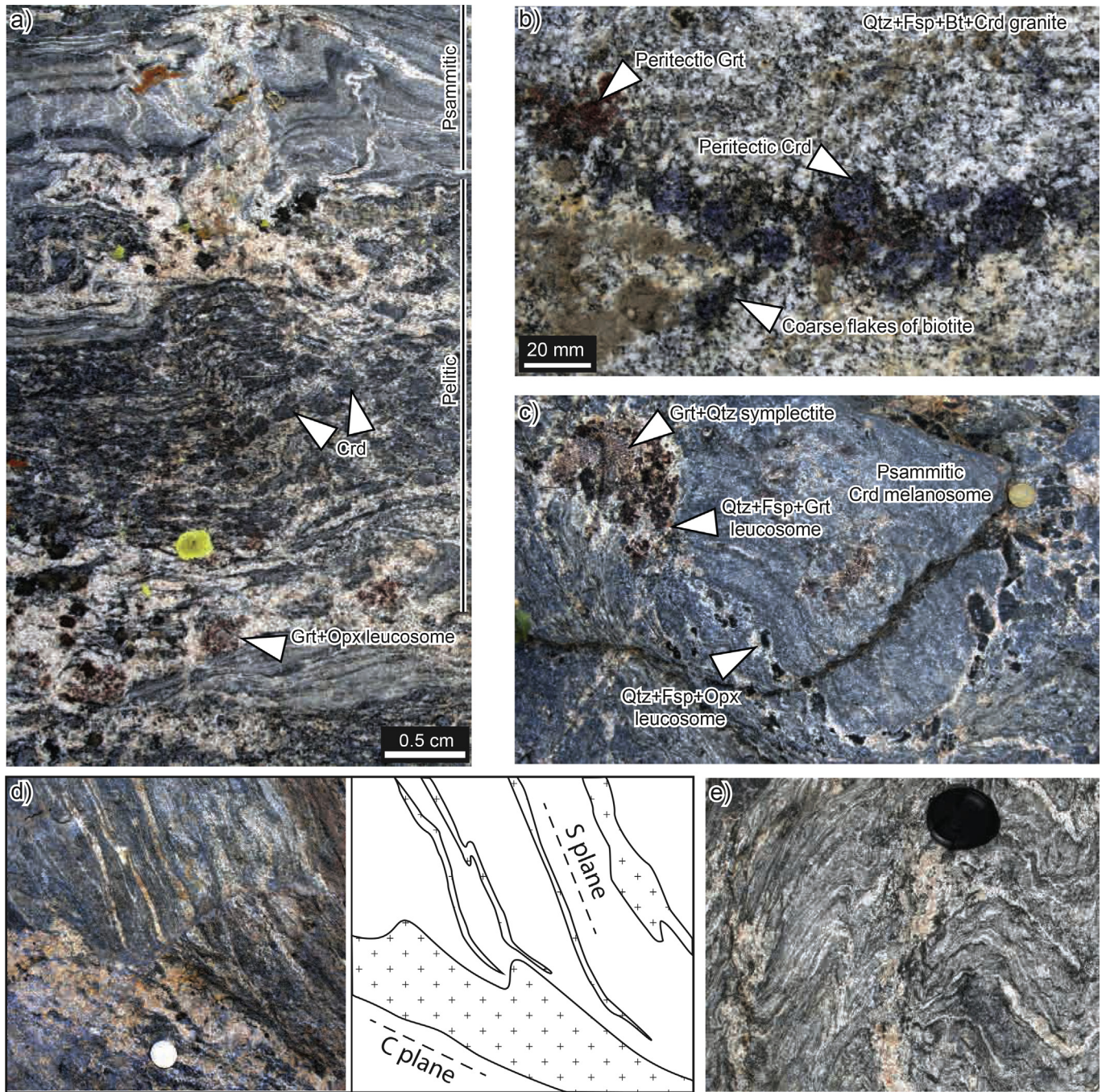


Fig. 4. Primary anatectic structures in weakly deformed Tolombón complex migmatites, protoliths to the PSZ mylonitic rocks. (a) Metatexite with compositional layering inherited from the interbedded protolith which controls leucosome composition and volume. Leucosomes intrude into and cut across foliation in top psammitic layer. (b) Peritectic Crd and Grt porphyroblast aggregates rimmed by biotite inside a Qtz+Kfs+Pl+Bt+Crd granite. Biotite rims are interpreted to result from retrogression due to reaction with crystallizing melt. (c) Patchy Grt–Opx leucosomes with Grt+Qtz symplectite in psammitic Crd–melanosome. (d) Leucosomes in thrust planes indicating possible involvement of melt during thrusting (line drawing shows interpretation of structures). (e) Leucosomes on axial planes of folds formed during shortening related to thrusting event, indicative of syn-kinematic anatexis. (a–d) are vertical planes, parallel to stretching lineation and perpendicular to foliation, (e) is perpendicular to the axial plane of folds.

proportion of protomylonitic metatexite is more than 50% of the total outcrop.

3.2. Protomylonitic metatexite

Protomylonitic metatexites (Fig. 5a) outcrop in Anchillo river gorge and form a 1 km thick-layer at the top of the PSZ. They are differentiated from the weakly deformed rocks NE of the PSZ (Fig. 4) by a higher proportion of dark grey recrystallized matrix

and increased foliation intensity. The latter is indicated by an increase in the alignment of micas and the stretching and flattening of quartz and feldspar phenocrysts (Fig. 5a). Quartz and feldspar phenocrysts in the stromatic metatexite become porphyroclasts in the protomylonite and the mica-rich matrix is deflected around them forming S–C fabric. Many porphyroclasts in melanocratic layers are elongate parallel to the foliation or form σ - and δ -clasts with asymmetric tails that thin and recrystallize distal to the clast, but some porphyroclasts retain their euhedral tabular shape.

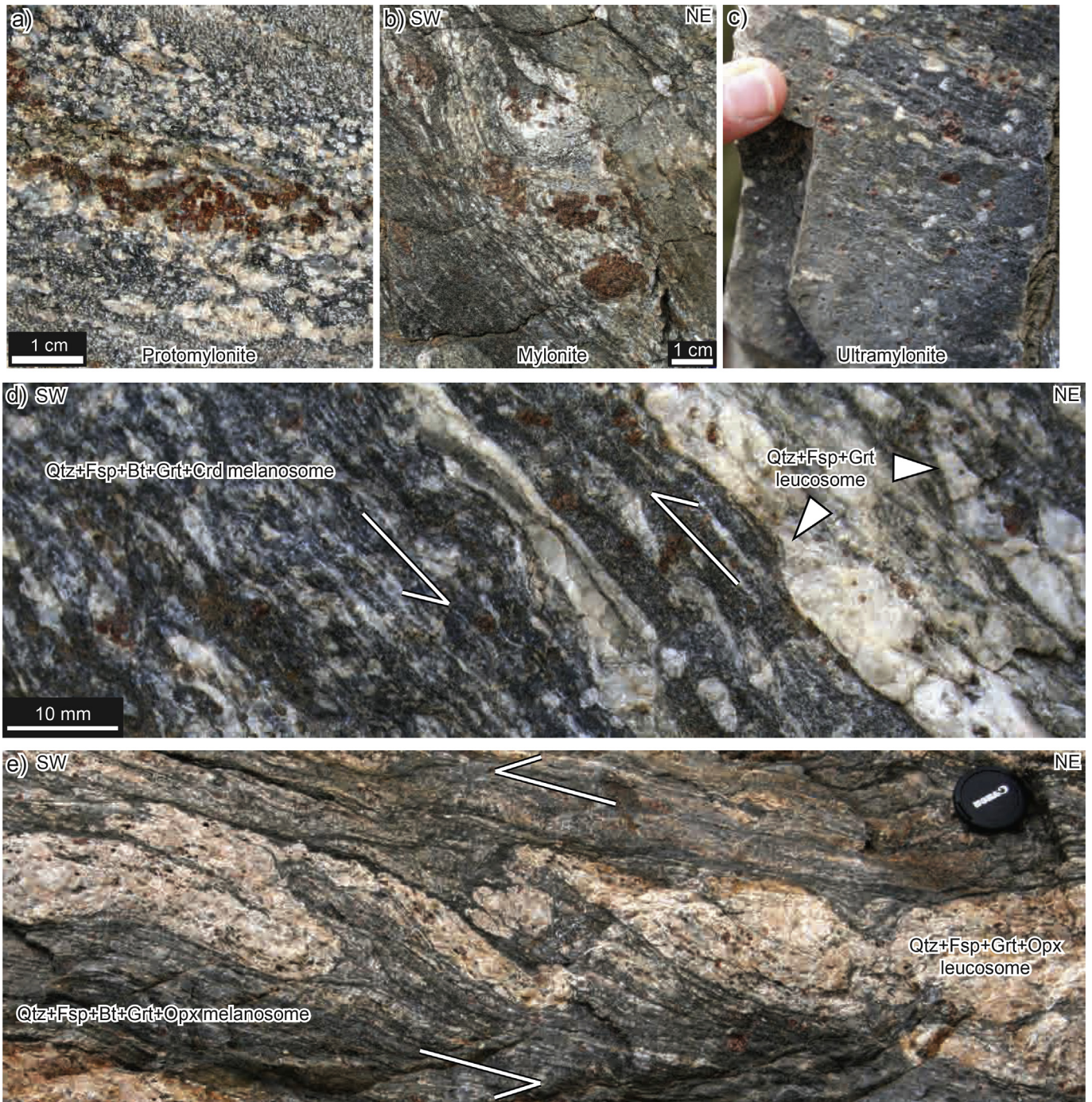


Fig. 5. Features of weakly to highly sheared rocks in metatexite layers of the PSZ. (a) Garnet aggregate in protomylonitic metatexite. (b) Large garnet grains in relict leucosome that has been asymmetrically sheared into a lens indicating top-to-SW shear in a mylonitic metatexite. (c) Ultramytonitic metatexite with naked and rounded clasts of garnet and feldspar. (d) S–C fabric and σ -clasts of feldspar indicating top-to-SW shear in Grt+Crd protomylonitic–mylonitic metatexite. (e) Asymmetric SW-verging folds of Grt+Opx leucosome and melanosome in mylonitic metatexite. All planes are parallel to stretching lineation and perpendicular to foliation.

Leucosomes are generally continuous with their boundaries parallel to S–C fabric but show little obvious internal deformation. Primary anatectic structures described in Section 3.1 are still recognizable. Calc-silicate nodules present in this layer are up to 2 m long and elongate parallel to the foliation.

Within this layer of protomylonitic metatexite there are discontinuous layers of mylonitic metatexite (Fig. 5b,d,e; described in Section 3.3). These increase in proportion to the SW until they form greater than 50% of the total outcrop marking a subjective boundary with the top of the mylonitic metatexite.

3.3. Mylonitic metatexite

The main difference between mylonitic and protomylonitic metatexites is the proportion of mylonitic layers. Mylonites are characterized by a higher proportion of dark grey, fine-grained, recrystallized matrix (Fig. 5b,d,e). Leucosomes and melanosomes are still recognizable and show the same mineralogy and calc-silicate nodules are approximately the same shape and size. Marking the increased strain, leucosomes are sheared into asymmetric, disrupted lenses (Fig. 5b) or folded asymmetrically and

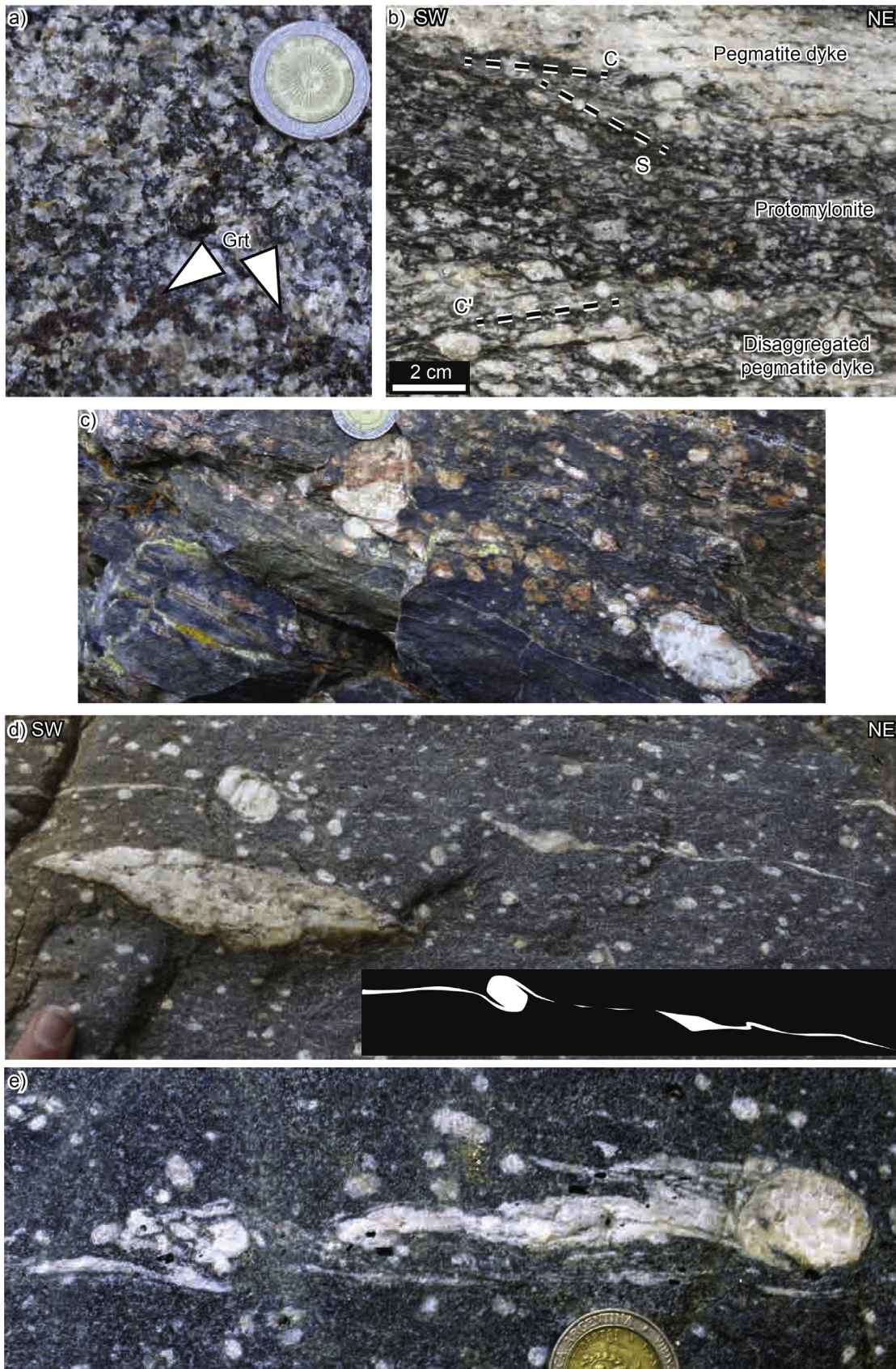


Fig. 6. Features of weakly to highly deformed rocks in the ultramylonitic diatexite layer of the PSZ. (a) Granitic diatexite from a preserved low strain lithon. (b) Progressive disaggregation of pegmatite dyke (top) forms disconnected dykelets and large clasts (bottom) and eventually discrete porphyroclasts (middle) in a protomylonite. (c) Mylonitic pegmatite dyke with large K-feldspar grains. (d) δ -clast (top) and σ -clast resulting from shearing of pegmatite dyke in ultramylonitic diatexite. (e) K-feldspar porphyroclast with “comet” tail and smaller naked porphyroclasts in ultramylonite (view down plunge of stretching lineation). (f) Finely interlayered garnet-bearing gneiss, protomylonite and

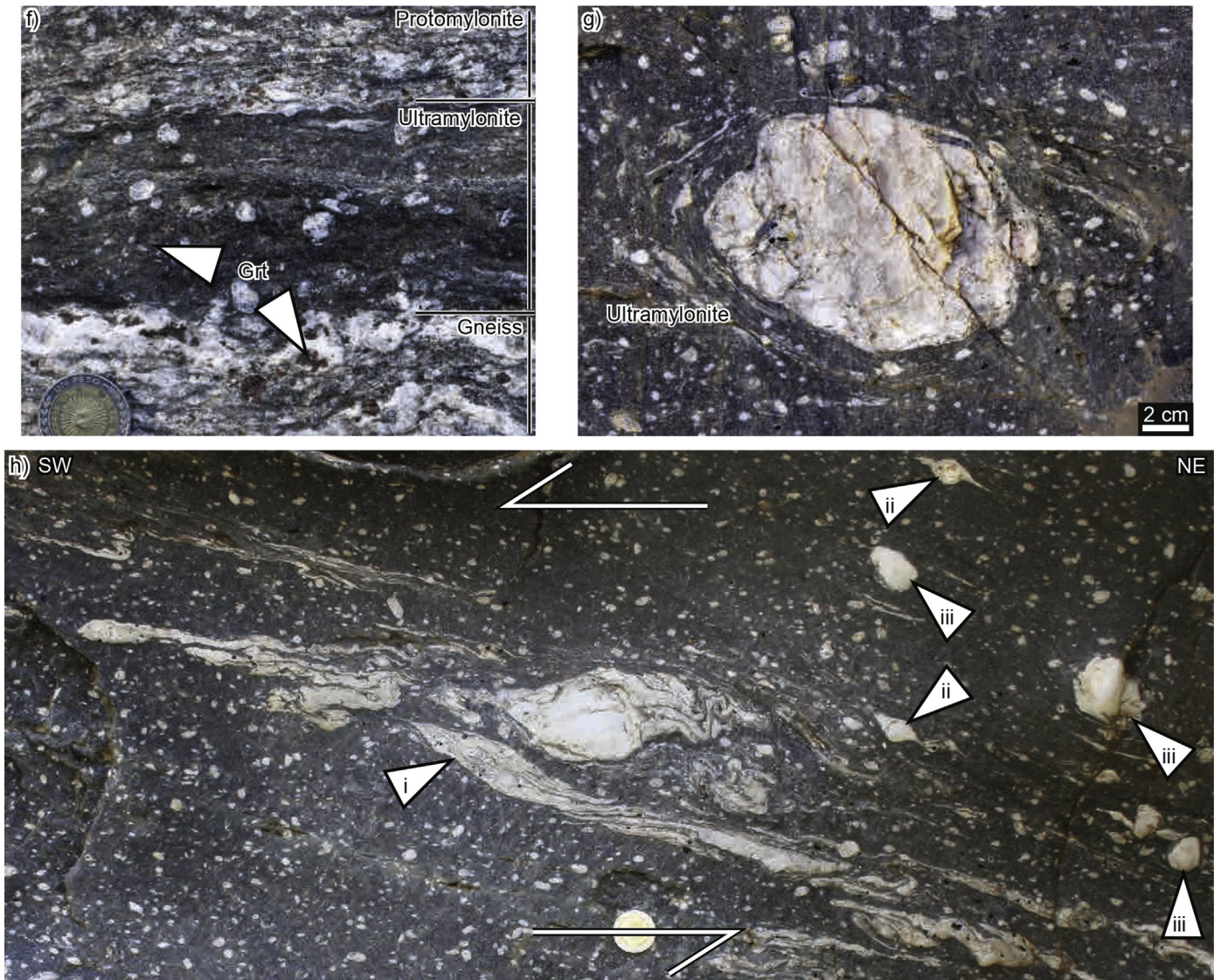


Fig. 6. (continued).

intensely (Fig. 5e), indicating their higher viscosity in comparison to melanosome. In melanocratic layers the intensity of the foliation is greater, S–C fabric is well developed, and porphyroclasts of feldspar form σ - and δ -clasts with short asymmetric tails (Fig. 5b,d). Garnet, cordierite, and orthopyroxene in melanocratic layers are surrounded by remnant leucosomes that are asymmetrically sheared (Fig. 5b). Primary anatectic structures are partially preserved, limited to coarse flakes of biotite rimming peritectic minerals, occasional tabular feldspar porphyroclasts, and symplectitic intergrowths of garnet and quartz.

The mylonitic metatexites form a 1.5 km-thick layer that contains occasional and discontinuous layers of protomylonitic (Fig. 5a) and ultramylonitic metatexite (Fig. 5c). Ultramylonitic rocks form melanocratic layers a few cm wide that contain >90% recrystallized matrix and naked, rounded porphyroclasts of feldspar, garnet

(Fig. 5c), cordierite, and orthopyroxene. Below the 1.5 km layer of mylonitic metatexite there is a gradational contact with the underlying layer of much more massive ultramylonitic diatexite (Fig. 6).

3.4. Ultramylonitic diatexite

We first describe the features of this ultramylonitic layer, before describing the transition from the mylonitic metatexites above and these ultramylonites.

The mylonitic metatexite layer grades downward into a massive, homogenous ultramylonitic rock consisting of rounded feldspar porphyroclasts in a black matrix (Fig. 6) that forms a 1 km-thick layer at the base of the PSZ (Fig. 2). Locally the matrix is dark green from retrogression of biotite to chlorite and in some regions the proportion of recrystallized matrix gradually decreases with a

ultramylonite. (g) Large K-feldspar porphyroclast disaggregated from a pegmatite dyke and rotated in ultramylonitic matrix during shearing, causing high rotational strain on its margins and circumcentric ribbons of recrystallized feldspar (view down plunge of stretching lineation). (h) Pegmatite sheared in ultramylonite forming asymmetric lenses (i), σ -type clasts (ii), and, through prolonged rolling and rotation in the matrix, θ -type clasts (iii). View in all photographs except for (e) and (g) is parallel to stretching lineation.

concomitant increase in the proportion of porphyroclasts until a homogenous porphyritic granitic diatexite can be recognised (Fig. 6a). From this association, we interpret that the protolith to the ultramylonites was a granitic diatexite and we call this layer ultramylonitic diatexite.

Within these ultramylonites, there are discontinuous quartz-feldspar layers that contain large feldspar crystals (up to 20 cm in diameter), interpreted as sheared and disaggregated pegmatite dykes. These rocks also document the gradual disaggregation of dykes into σ -clasts (Fig. 6d,h), and then into naked porphyroclasts (Fig. 6g). There are occasional thin (0.5–15 m wide and a few hundred metres long) lenses of protomylonitic diatexite (7% of total width of the 1 km ultramylonitic layer) and mylonitic diatexite (13% of total; Fig. 2) recognized by the lower modal proportion of recrystallized matrix, generally coarser grain size, increased preservation of euhedral feldspars and other primary structures, and less strained, continuous pegmatites. In contrast to the mylonitic metatexites, none of the rocks are layered (Fig. 6) and calc-silicate nodules are absent.

The top of the layer of ultramylonitic diatexite contains porphyroclasts of garnet (Fig. 6f) which reduce in proportion and size downward to the SW, becoming absent 400 m from the base. Immediately below where garnet becomes absent there is a 200 m thick zone where ultramylonites are overprinted by brittle structures (between SQ179 and SQ180; Figs. 2 and 3) described in Section 6. Below the brittle fault zone there is a return to the massive ultramylonitic diatexite for 200 m until the contact with the underlying meta-psammite and -pelites of the Agua del Sapo complex (Fig. 2).

3.5. Transition into ultramylonitic diatexite

The transition from the overlying layer of mylonitic metatexite (Section 3.3) to the ultramylonitic diatexite is described in two regions with complementary information: the southern and northern transects (Fig. 2).

The southern transect is characterized by a gradual transition that is well preserved in a low strain lithon where we recognize many protolith features. Approaching this lithon from the NE to the SW, there is an increase in leucocratic layers in the mylonitic metatexite with a concomitant decrease in the intensity of foliation until melanocratic layers become absent, and the rock becomes a porphyritic granitic diatexite that preserves a granitic texture with psammitic and pelitic schollen (Fig. 6a; at point SQ183 in Fig. 2). Further to the SW this low strain lithon of diatexite transitions into mylonites over a region ~60 m wide where strain intensity increases. This is marked by an increase in the intensity of foliation and definition of S–C fabric and a gradual decrease in the proportion of feldspar porphyroclasts (phenocrysts in the granitic diatexite) and in the size and proportion of garnet.

Within this sequence there is a 20 m-thick layer of a rock that consists mostly of K-feldspar with crystals up to 5 cm in diameter with small garnets (<2 mm diameter), and strongly stretched ribbons of quartz and feldspar. This rock is interpreted to be a mylonitic–ultramylonitic pegmatite and in places the matrix is dark grey and recrystallized and contains few rounded porphyroclasts of K-feldspar (Fig. 6c).

Unlike the southern transect, the northern transect does not include preserved lithons of weakly deformed diatexite. Instead the mylonitic metatexite transitions directly into a massive ultramylonite of the kind described in Section 3.4 and interpreted to have formed after granitic diatexite. As in the southern transect, the northern transect contains garnet 1–6 mm in diameter (Fig. 6f) that occurs in aggregates and decreases in proportion to the SW. The northern transect also contains pegmatite dykes which transition

into a rock with large K-feldspar porphyroclasts sheared into σ - and δ -clasts surrounded by dark grey matrix interpreted as mylonitic–ultramylonitic pegmatite (Fig. 6c). In contrast to the southern transect, here pegmatite dykes are thinner forming only metre-thick bands.

3.6. Contact with the footwall of the PSZ

At the base of the ultramylonitic diatexite layer there is an abrupt change to an interbedded rock that contains layers of meta-sandstone comprised of quartz, K-feldspar, plagioclase, biotite, and garnet that alternate with layers of finer grain size meta-mudstone that contain biotite, K-feldspar, quartz, plagioclase, muscovite, and garnet. This layering is interpreted to be sedimentary in origin indicating a change in rock type from the homogenous, massive ultramylonitic diatexite to sheared interbedded meta-psammite and -pelite. The pelitic layers commonly form well-foliated schists and the sequence contains calc-silicate nodules and layers. There are no primary anatectic structures like those in the Tolombón complex, indicating the rock is part of the amphibolite facies Agua del Sapo complex.

The metasedimentary rocks contain pegmatite dykes that are sheared into discontinuous lenses and large (up to 25 cm diameter) porphyroclasts, similar to dykes in the ultramylonitic diatexites. Within these rocks are layers where the matrix becomes very fine-grained and biotite-rich, and porphyroclasts are rounded and naked. These layers are interpreted as ultramylonitic metasedimentary layers and still part of the PSZ. Further south, garnet–cordierite bearing interbedded meta-psammite and -pelite do not contain mylonitic layers and while pegmatite dykes are sheared, they are generally continuous. These rocks are interpreted to be outside of the high strain zone and accordingly their appearance mark the base of the PSZ (Fig. 2).

4. Structures

In this section we present the full range of structures in the shear zone. We focus first on structures in weakly deformed through to ultramylonitic metatexites (Section 4.1) and then on structures preserved in the 1 km-thick ultramylonitic diatexite layer at the base of the PSZ (Section 4.2).

4.1. Structures in deformed metatexites

This layer shows a gradual transition from weakly deformed and gneissic metatexites into mylonitic rocks. We describe the structures in weakly deformed rocks first and then the changes as strain increases.

Weakly deformed metatexites in the hanging wall of the PSZ show bedding-parallel foliation that dips moderately SE or NE (Fig. 1b; mean = 115/46; measurements in dip direction/dip) with a SE-plunging stretching lineation (mean = 138/34). The foliation, defined by micaceous planes consisting dominantly of biotite, is well-developed in pelitic layers but weak in psammitic layers (Fig. 4a). Leucosomes are generally foliation parallel in pelitic layers but in psammitic layers form isolated patches that are not foliation parallel or intrude from pelitic layers and cross cut foliation (Fig. 4a). Leucosomes are also found in shear planes, commonly sub-parallel to the axial plane of folds and these features are interpreted as indicative of syn-kinematic melting (Fig. 4d,e).

The foliation in the protomylonitic metatexite is defined by the same features as in less deformed metatexites but it is better developed and dips moderately ENE (mean foliation in protomylonitic and mylonitic metatexites = 73/41) with stretching lineations that plunge moderately to the east (mean lineation = 92/

39; Fig. 2). Thrusting with top-to-W transport direction is indicated in protomylonitic metatexites by asymmetric shearing of leucosomes into σ -shaped lenses or σ -shaped porphyroclasts (Fig. 5a), S–C fabric in the melanosome, asymmetrically folded leucosomes, and garnet, cordierite, and orthopyroxene porphyroclasts with asymmetric strain shadows of biotite, quartz and feldspar. Garnet aggregates are occasionally sheared into σ -type shapes. Calc-silicate nodules are flattened parallel to the foliation and may have stair-stepping tails. Leucocratic bands are parallel to both S and C planes and show pervasive internal deformation indicative of solid-state deformation after anatexis ceased. The relationship between anatexis and shearing is discussed further in Section 8.1.

Mylonitic metatexites have more intensely developed foliation (Fig. 5b) with thicker and more continuous layers of biotite defining S–C fabric. Structural features are the same as for protomylonites but leucosomes are less continuous and a greater proportion are sheared into σ -shaped lenses (Fig. 5b) and asymmetrically folded with SW vergence (Fig. 5e). Inside these mylonites there are thin layers of melanocratic ultramylonitic layers characterized by rounded naked clasts of feldspar, garnet, cordierite, and orthopyroxene in a fine and dark matrix. Clasts are generally smaller than those in protomylonites and mylonites (Fig. 5c) with very few σ -clasts, σ -shaped lenses of leucosomes, or asymmetric folds.

4.2. Structures in deformed diatexites

The homogeneity of the diatexite protolith and the intrusion of pegmatite dykes into the layer of ultramylonitic diatexite caused the development of structures that are different to those in the layer of mylonitic metatexite. Within the layer of ultramylonitic diatexite the thin layers of protomylonite and mylonite show similar structures to the ultramylonite so they are discussed together with any differences highlighted.

Similar to the attitude of the foliation in the protomylonitic and mylonitic metatexites, foliation in the layer of ultramylonitic diatexites dips moderately to the east (mean = 83/41) with an east-plunging stretching lineation (mean = 91/39; Fig. 2). In the northern transect (Section 3.5) the foliation rotates gradually from NE to SE dipping defining a broad fold (Fig. 2). The intersection of these planes defines a fold axis which plunges moderately to the east, approximately parallel to the stretching lineation, indicating folding could be a result of large-scale undulations of thrust planes.

The large clasts from sheared pegmatite dykes show a range of structures related to variable amounts of rotation. Porphyroclasts that have experienced little rotation show asymmetric tails and pressure shadows, form σ -type clasts (Fig. 6d,h) and occasionally have comet-like tails (Fig. 6e). With increasing rotation δ -type clasts are produced (Fig. 6d,h) or porphyroclast tails wrap around and mantle the clast (Fig. 6g). These structures are more common in protomylonitic and mylonitic diatexites than ultramylonitic diatexites. The ultimate product of this rotation is naked θ -type clasts characteristic of ultramylonites, possibly because of shearing, thinning, and complete recrystallization of porphyroclast tails (Fig. 6g).

Similar to the mylonitic metatexites, this layer contains occasional tabular porphyroclasts of feldspar, asymmetric shearing of garnet aggregates, and S–C fabric in biotite-rich layers. These features are more pronounced in mylonites than protomylonites but less apparent in ultramylonites which are dominated by naked clasts and strongly sheared pegmatite dykes.

5. Microstructures

Here we start with the description of primary anatectic microstructures (Section 5.1) and then describe the secondary

microstructures of mylonitic metatexites (Section 5.2) and diatexites (Section 5.3). The microstructures at each level of the PSZ share a broadly similar set of features characteristic of deformation at amphibolite facies. Grain sizes were determined using digitised maps of 300 grains which were analysed for average grain size using the median Feret diameter (N. Hunter, pers. communication).

5.1. Primary anatectic microstructures

Primary anatectic microstructures are evident in weakly deformed and protomylonitic metatexites in the NE of the PSZ. These microstructures are largely absent in ultramylonitic metatexites but occasionally preserved in mylonitic metatexites.

Leucosomes consist of Qtz+Kfs+Pl+Grt±Crld±Sil±Opx and melanosomes of Bt+Sil±Crld±Ky±Grt±Ilm±Mag±Rt±Ap±Mnz±Ms (Fig. 7a) with increasing proportions of quartz and feldspar closer to leucosomes. In melanosomes anhedral quartz grains are interstitial to biotite and feldspar. Feldspar occasionally forms euhedral tabular crystals that are interpreted as igneous in origin, and plagioclase commonly shows lamellar crystallisation twins, or two sets of twins perpendicular to each other (Fig. 7b).

In weakly deformed metatexites peritectic minerals are found dominantly in leucosomes. There are two types of sillimanite: Sil1 occurs in leucosomes fringing the boundaries of large feldspar crystals (Fig. 7a), and is interpreted to be peritectic. Sil2 and Bt2 replace cordierite (Fig. 7a,b) and garnet, and are interpreted to be a result of the reaction of garnet and cordierite with melt during crystallization (Büttner et al., 2005; Sawyer, 2008). When replacing cordierite, Sil2 is occasionally accompanied by kyanite which forms small subhedral porphyroclasts that show random orientation with respect to the foliation (Fig. 7a) indicating that deformation ceased before the stability field of kyanite was reached, following the interpretation of Büttner et al. (2005).

Garnet is 0.5–30 mm in diameter and commonly poikiloblastic with biotite-filled fractures and inclusions of bulbous quartz, coarse biotite, euhedral zircon, and occasional wormy intergrowths of ilmenite. All inclusions are generally larger than the size of the same mineral in the matrix. In some cases garnet is surrounded by orthopyroxene and in such instances garnet contains wormy intergrowths of quartz forming symplectite (Fig. 7d; Waters, 2001). In areas with a high proportion of biotite and garnet, ilmenite is common and contains exsolved magnetite.

Cordierite is anhedral and up to 5 mm in diameter (Fig. 7a,b). It appears in leucosomes and melanosomes and is the most abundant mineral in some restitic migmatites. It is poikiloblastic with inclusions of quartz, biotite, and zircon and sometimes has an inclusion-free mantle surrounding a poikiloblastic core. Cordierite contains discontinuous lenticular twins and alteration to white mica on microfractures.

Orthopyroxene occurs only in leucosomes and forms large (up to 40 mm), anhedral, occasionally poikiloblastic grains that contain inclusions of quartz, biotite, and ilmenite with magnetite exsolution (Fig. 7c,d). It is replaced at its margins by biotite and occasionally garnet (Fig. 7c). Biotite is partially replaced by chlorite due to a later retrogression.

5.2. Deformation microstructures in sheared metatexites

The deformation microstructures are described for protomylonitic metatexites and differences in mylonitic and ultramylonitic metatexites are then highlighted. Although metatexites show a general decrease in grain size from protomylonites to ultramylonites, grain size estimates are not provided because the variation is too large due to the presence of heterogeneous

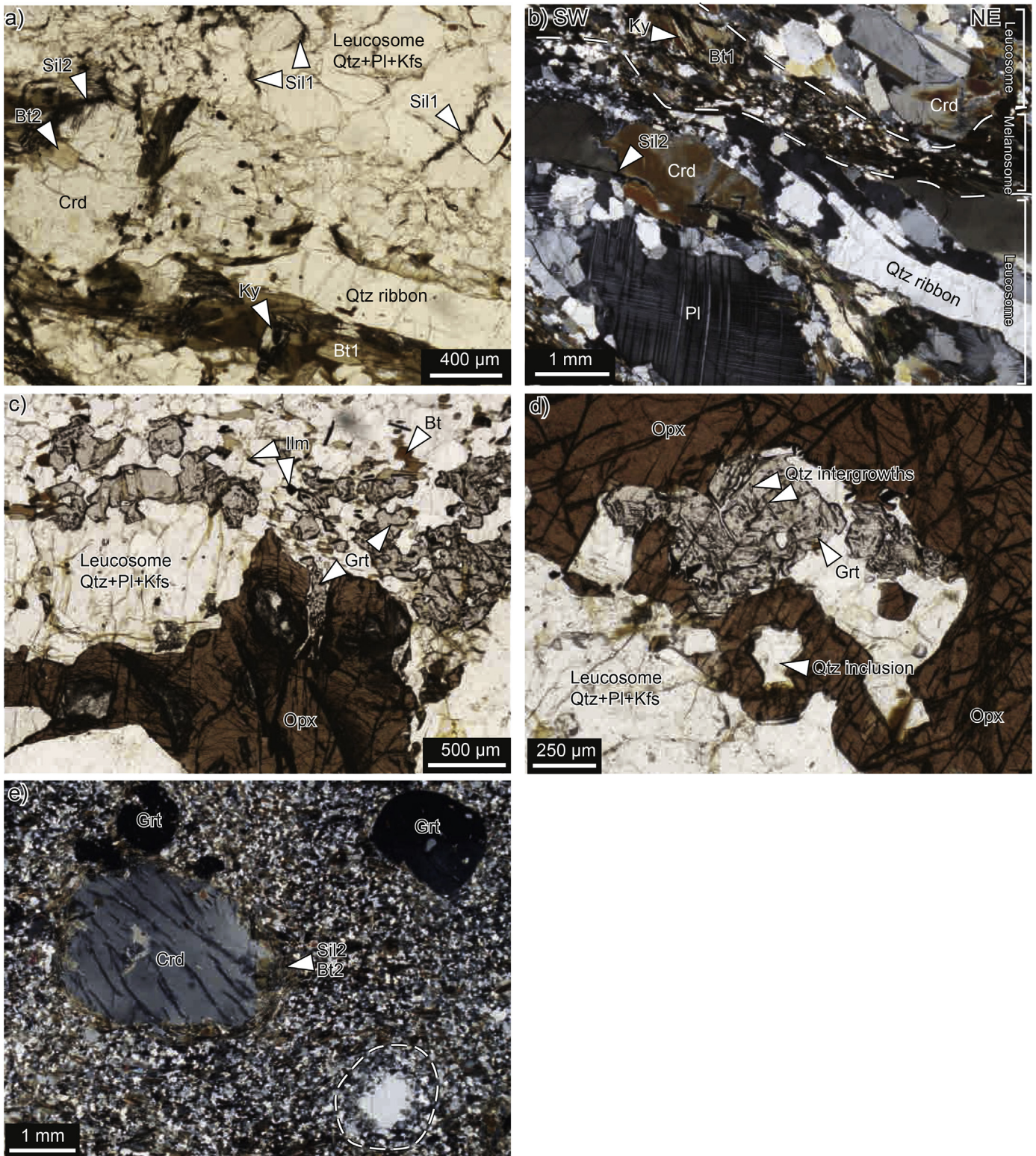


Fig. 7. Metamorphic and microstructural features of deformed rocks after metatexites. (a) Leucosome containing peritectic sillimanite (Sil1) in a Crd-melanosome with kyanite and sillimanite (Sil2; plane polarized light, PPL). (b) Leucosomes and melanosome in metatexite. Quartz in leucosomes is polygonal (top right) or forms ribbons that wrap around peritectic cordierite and plagioclase. Plagioclase contains two sets of twins and shows recrystallization on foliation parallel boundaries. Cordierite is partially replaced at margins by sillimanite (Sil2) and biotite (Bt2). Biotite-rich melanosome contains porphyroblasts of kyanite and interstitial quartz and feldspar (crossed polarised light, XPL). (c) Orthopyroxene–garnet leucosome. Garnet partially replaces orthopyroxene, Bt+Ilm partially replaces garnet (PPL). (d) Orthopyroxene with inclusions of garnet and quartz. Garnet inclusion contains wormy intergrowths of quartz (PPL). (e) Ultramylonite showing fine-grained matrix with poorly-developed foliation and rounded cordierite, garnet, and feldspar porphyroclasts. Cordierite rim is partially replaced by Bt2 and Sil2 and plagioclase has a recrystallised mantle (dashed line; XPL). All thin sections are cut parallel to stretching lineation, perpendicular to foliation.

leucocratic and melanocratic bands and abundant porphyroclasts of garnet, cordierite, and orthopyroxene which do not recrystallize.

Quartz ribbons and leucosomes in protomylonitic metatexites form continuous bands that, together with the micaceous bands, are parallel to S–C fabric and deflect around porphyroclasts (Fig. 7b). Feldspar porphyroclasts occasionally retain crystallization twins (Fig. 7b) and euhedral tabular shape but more commonly show sweeping undulose extinction, recrystallization at margins, and have asymmetric strain shadows with recrystallised quartz and feldspar forming δ - and σ -clasts. Feldspar contains late patchy sericitisation and occasionally microcracks parallel to cleavage planes. Myrmekite is present on some K-feldspar faces parallel to the foliation. Muscovite fish are common and show stair-stepping wings. Quartz in leucosomes has a polygonal shape indicating recrystallization at moderate temperatures, and quartz ribbons are >5 cm long and contain grains of variable sizes with lobate boundaries and pinning structures (Fig. 7b), interpreted to indicate grain boundary migration (GBM) recrystallization indicative of regime 3 of Hirth and Tullis (1992).

In mylonitic metatexites the well-developed S–C fabric is defined by quartz ribbons, biotite and sillimanite, and alignment of leucosome boundaries (Fig. 7a,b). Quartz has the same appearance as in protomylonitic metatexites and it also shows GBM but quartz ribbons are shorter, ~5 mm long, and deflect around porphyroclasts (Fig. 7b).

Ultramylonitic metatexites have a weakly foliated matrix of uniform grain size (Fig. 7e). Unlike protomylonitic and mylonitic metatexites, layers of biotite are ill-defined and instead biotite appears dispersed in the matrix (Fig. 7e). Feldspars have recrystallized margins forming core-and-mantle structure and show late sericitisation (Fig. 7e). Quartz ribbons showing GBM are rare and much shorter than in mylonitic metatexites, crystallization twins in feldspar porphyroclasts are uncommon, and σ - and δ -clasts are absent.

5.3. Deformation microstructures in sheared diatexites

As mentioned in Section 4.2, the homogeneity and presence of pegmatite dykes in the ultramylonitic diatexites gave rise to structures absent in sheared metatexite. Here we focus only on those microstructures which are different. While the layer is dominantly ultramylonitic (as described in Section 3.4) it also contains protomylonitic and mylonitic layers and these are described first, and then compared to ultramylonitic rocks to document the gradual increase in strain. Like for sheared metatexites, these rocks also record deformation at amphibolite facies conditions with late greenschist, possibly static overprint.

Protomylonitic diatexites contain a matrix of Qtz+Kfs+Pl+Bt±Ms±Chl±Sil±Ap with an average quartz grain size of $95 \pm 20 \mu\text{m}$ and an average mica grain size of $170 \pm 60 \mu\text{m}$. Porphyroclasts of K-feldspar and plagioclase are tabular to rounded with occasional inclusions of coarse flakes of biotite and muscovite and rare monazite (Fig. 8a). Muscovite inclusions are aligned parallel to crystallographic planes of feldspar porphyroclasts (Fig. 8a). Crystallization twins are evident in some feldspar porphyroclasts. Porphyroclasts in protomylonitic diatexite show partial recrystallization, similar to those in the mylonitic rocks of the metatexite but with a higher degree of recrystallization and a progression from core-mantle structure, through to completely recrystallized porphyroclasts (Fig. 8b,c). They also show rotation without internal deformation to form naked clasts although this is rare and most porphyroclasts have strain shadows. The foliation is defined by aligned biotite grains that form connected layers that wrap around the porphyroclasts (Fig. 8a–c). Quartz ribbons show GBM and are a similar length to protomylonitic metatexites (Section 5.2) but also

wrap around porphyroclasts and occasionally form rootless isoclinal folds (Fig. 8a,c). Myrmekite occurs on some porphyroclast grains on foliation-parallel boundaries. Evidence for porphyroclast rolling includes δ -clasts and quartz ribbons that wrap around porphyroclasts (Fig. 8b,c,f) and either thin out or break up close to the porphyroclast (Fig. 8b–d).

Mylonitic diatexites have the same grain size as the protomylonites and contain quartz ribbons that are shorter than in the protomylonites, reaching lengths up to 10 mm but generally ~4 mm long, and are either continuous, parallel to foliation, or wrap around porphyroclasts (Fig. 8d). They do not show evidence for folding, unlike protomylonitic rocks, suggesting transposition. Compared to protomylonites, mylonitic diatexites contain a higher proportion of recrystallized matrix and naked and recrystallized porphyroclasts (Fig. 8d).

Ultramylonitic diatexites have an average quartz grain size of $60 \pm 10 \mu\text{m}$ and average mica grain size of $120 \pm 40 \mu\text{m}$ (Fig. 8e,f) and only a few small remnant porphyroclasts. These porphyroclasts are commonly rounded and have only weakly developed strain shadows or form naked clasts. In some cases they are completely recrystallized but retain the original shape of the porphyroclast (Fig. 8e) and were later partly sericitised and chloritised. Quartz ribbons are mostly absent but occasionally there are few aligned quartz grains that are coarser than the matrix and show remnant lobate boundaries. Unlike less deformed diatexites, connected planes of biotite are missing and instead, biotite is dispersed in the matrix. Consequently the foliation is not well developed (Fig. 8e,f cf. 8a–c).

5.4. Interpretation of microstructural data

Irrespective of whether the protolith was metatexite or diatexite, and independent of the intensity of shearing or position in the shear zone, all rocks record partial recrystallization of feldspar, GBM in quartz ribbons, and/or myrmekite on foliation-parallel planes. These features indicate that the temperature of shearing in all rocks and at all structural levels of the PSZ was in the range of 500–700 °C (Passchier and Trouw, 2005) above greenschist facies.

The change from protomylonites to ultramylonites for both protoliths is marked by an increase in the proportion of recrystallized matrix, a decrease in the proportion of porphyroclasts, together with a decrease in the grain size, and length and number of quartz ribbons (nearly absent in the ultramylonites). The foliation intensity increases towards mylonitic rocks but then decreases as rocks become ultramylonitic. In parallel, strain shadows and σ - or δ -clasts grow in importance towards mylonites but then are lost in ultramylonites, dominated by naked clasts.

While there are many microstructural commonalities between all sheared rocks within the PSZ, the increase in intensity of porphyroclast rolling from proto- to ultramylonites leads to some significant differences. Rolling causes folding of the quartz ribbons and tend to destroy them as well as mica layers. This, together with dissolution–precipitation of feldspars that may have been activated in the fine-grained ultramylonites, disperses mica through the matrix where it pins quartz and inhibits its recrystallization and recovery, explaining the origin of the homogenous, weakly foliated matrix in the ultramylonites (Figs. 7e and 8e,f).

6. Late brittle fault zone

The zone of brittle overprint that occurs in the ultramylonitic diatexite layer (Fig. 2) includes brittle faults, breccia, cataclasite and pseudotachylite associated with fault-related folds (Fig. 9). Breccia (>30 vol.% angular fragments of wall rock) and cataclasite (<30 vol.% angular fragments) contain clasts in a brown to black,

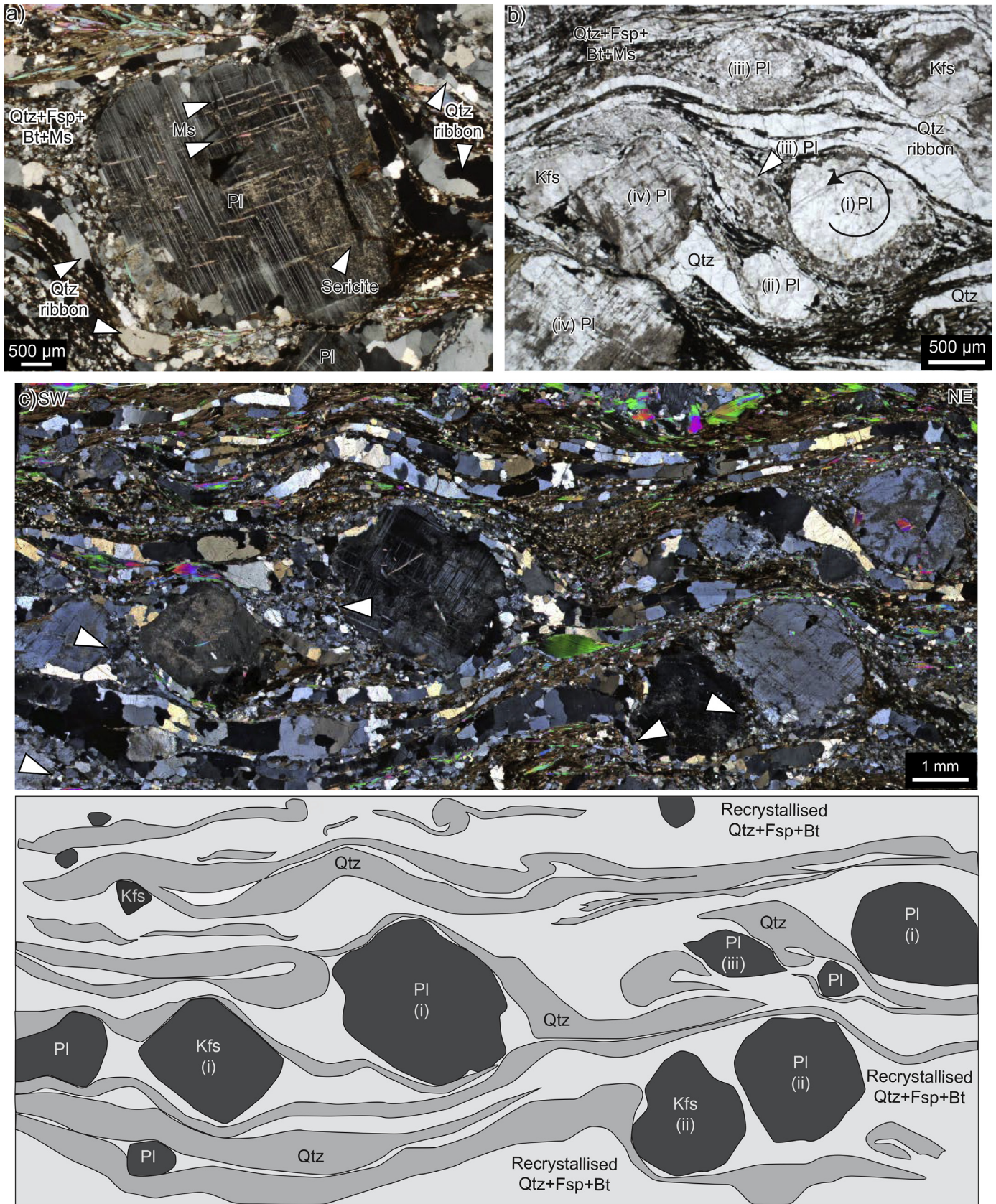


Fig. 8. Microstructures in deformed rocks after diatexites showing differences between protomylonites (a–c), mylonites (d), and ultramylonites (e,f). (a) Rounded plagioclase porphyroclast in protomylonite partially replaced by sericite with inclusions of muscovite parallel to twins. Quartz ribbons are longer than in mylonites and ultramylonites, wrap around the porphyroclast and show lobate boundaries and variable size indicating grain boundary migration (GBM) recrystallisation (XPL). (b) K-feldspar porphyroclasts in protomylonite show four different types of microstructure: rotation (grain i, indicated by circular arrow), partial (ii) to complete (iii) recrystallization, or are subhedral and sericitized

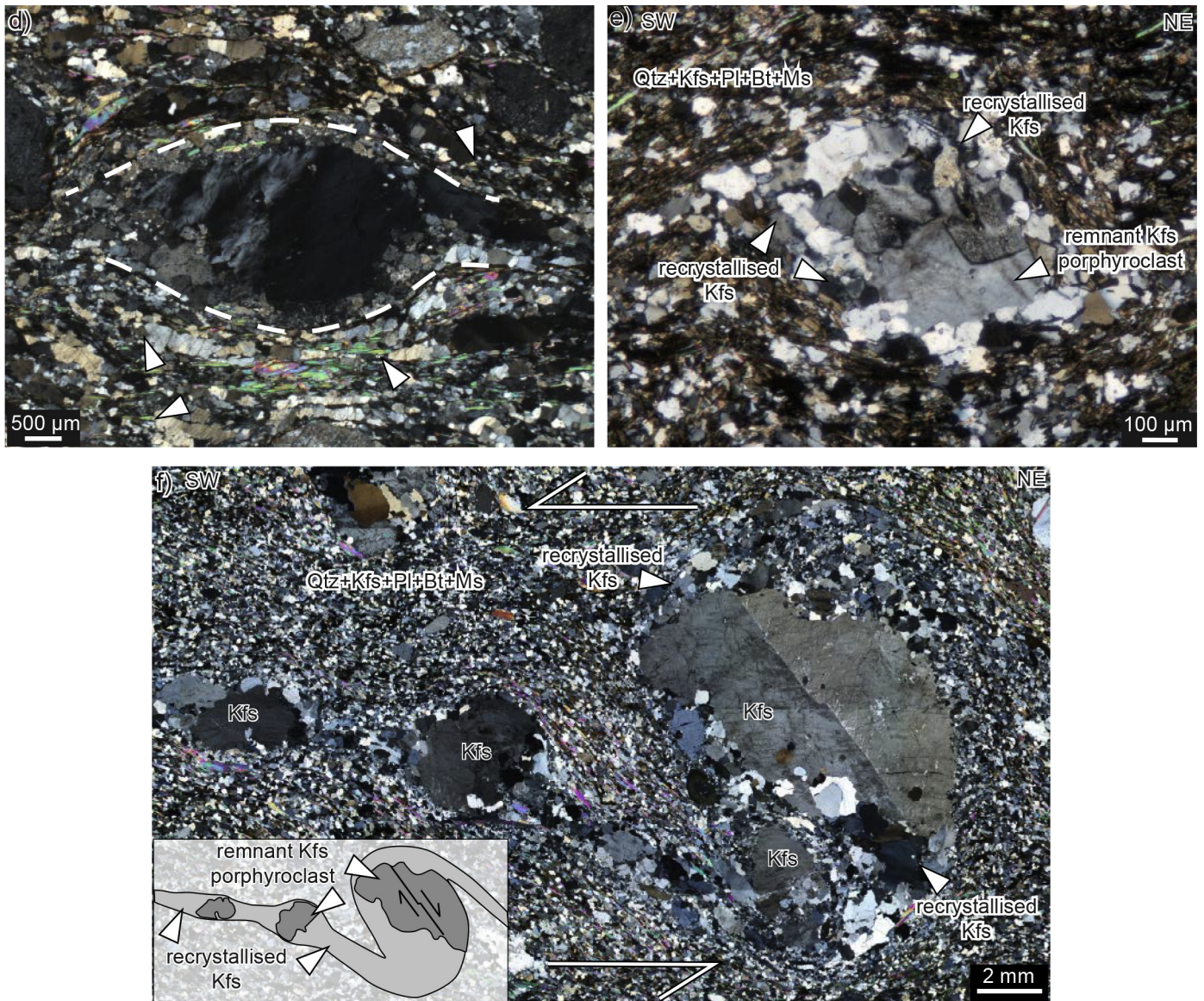


Fig. 8. (continued).

finely-comminuted, aphanitic matrix. The fragments contain single grains of quartz, feldspar, and muscovite and quartz ribbons which appear similar to those in the ultramylonitic host rock. Single grains of quartz and feldspar are up to 0.1 mm in diameter. In more altered rocks, feldspar is completely altered to very fine-grained sericite and larger grains are fractured with sericite concentrated on fractures. Biotite is absent from this region of brittle faulting.

Pseudotachylite consists of a black, aphanitic, glassy matrix with few fragments of wall rock or single grains of quartz and feldspar. The main generator vein is either foliation parallel or cross cuts the

foliation, and injection veins are common (Fig. 9b). The matrix in the pseudotachylite, breccia, and cataclaste is similar but in the pseudotachylite, the appearance of generator and injection veins with flow microstructures, suggests the matrix represents rapidly frozen silicate melt formed in the generator planes.

In the region of brittle faulting there are metre-scale folds that commonly occur close to fault planes. Folds are open and asymmetric with a mean fold axis of 162/30 (Fig. 2 inset) and axial planes defined by dissolution cleavage dip moderately south or east. The majority of fault planes dip moderately or steeply to the NE

(iv). The matrix is recrystallised and quartz ribbons wrap around porphyroclasts. Notice that a recrystallised ribbon of plagioclase wraps around feldspar clasts (e.g. centre grain, iii) showing the bi-modal behaviour of feldspar in protomylonites (PPL). (c) Protomylonite photomicrograph above and interpretative line drawing below: Most quartz ribbons are continuous and wrap around feldspar porphyroclasts which show rotation (i), and partial (arrows; ii) to complete (iii) recrystallisation. Quartz ribbons formed through high-temperature GBM are isoclinally folded in places (XPL). (d) Mylonite containing K-feldspar porphyroclast with recrystallised mantle (dashed lines) and an upper tail with sweeping undulose extinction. Unlike protomylonites, quartz ribbons pinch and swell and may be disaggregated into smaller, discontinuous ribbons (arrows; XPL). (e) Ultramylonite containing remnant K-feldspar porphyroclast core with recrystallised mantle. This mantle is misoriented from the remnant porphyroclast and subgrains are largely free of sericite (XPL). (f) Ultramylonite containing K-feldspar δ -clast showing top-to-SW shear sense. Tails are progressively disaggregated and recrystallised to form individual, isolated porphyroclasts. δ -clast shows brittle fracture along twinning plane, recrystallisation at margins, and rotation (XPL). Inset shows interpretation of microstructure.

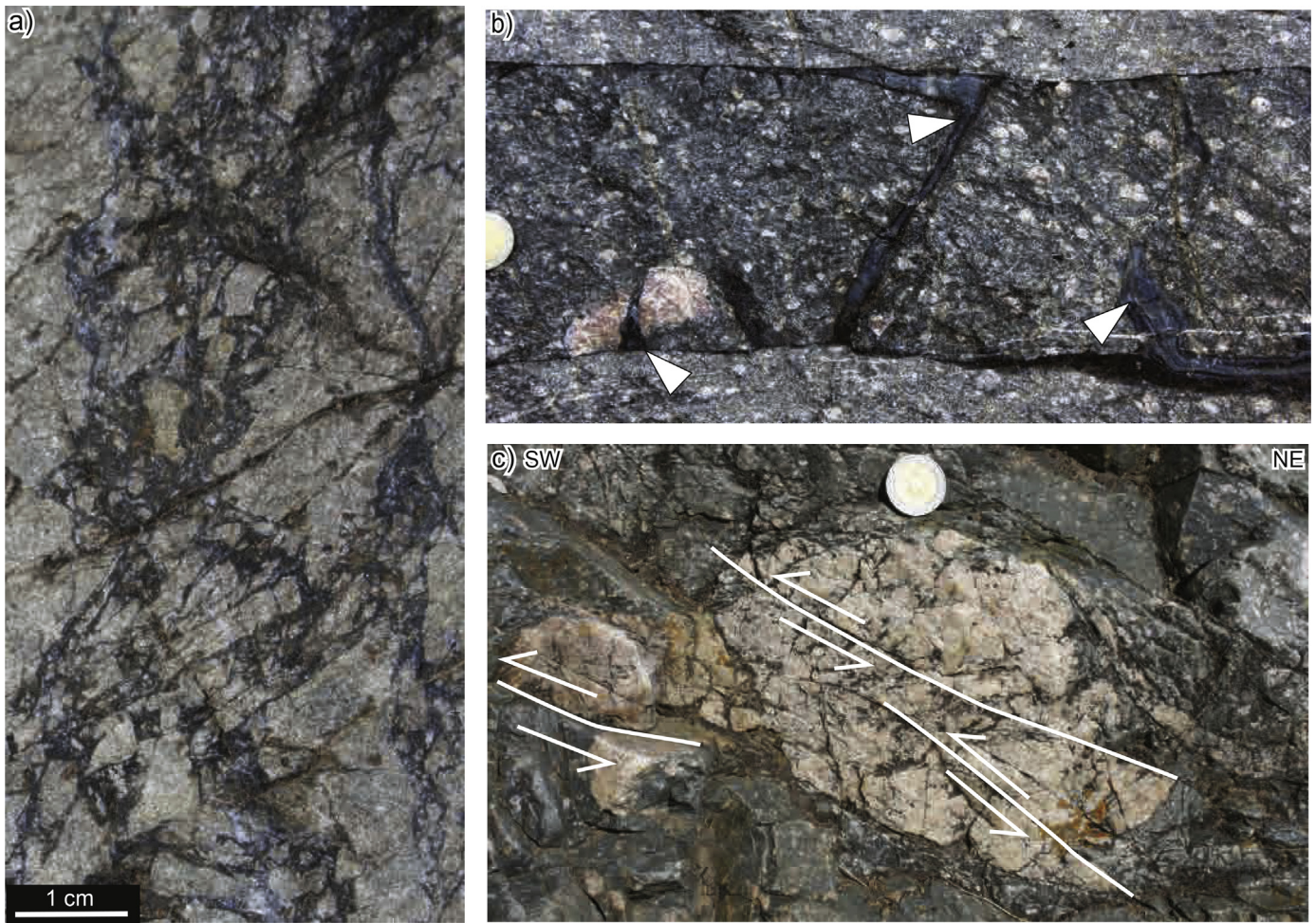


Fig. 9. Brittle overprint of ultramylonitic diatexites. (a) Ultramylonite altered and sericitised (lighter coloured rock), brecciated with cataclasite in fractures (darker rock). (b) Pseudotachylite in mylonitic diatexite. The horizontal planes are interpreted as generation surfaces and cross-cutting, glass-filled planes are injection veins (white arrowheads). In thin section glass, interpreted to represent frozen melt, is isotropic and contains flow structures and small, angular clasts. (c) Large clast from a pegmatite disaggregated during mylonitization and subsequently faulted. Note top-to-SW movement component.

although some dip SE or SW (Fig. 2 inset). While there is no discernible striation on the planes the faults consistently show thrust shear sense indicating thrusting generally to the WSW (Fig. 9c). On the stereonet the poles to the fault planes that are associated with the folds define a great circle indicating a common line of intersection at 140/34, not far from the average orientation of the fold axes. This is interpreted as the intermediate stress axis, σ_2 , during faulting (Fig. 2 inset). σ_1 and σ_3 are on the great circle and are poorly defined because of the absence of a striation but we estimate σ_3 as plunging moderately W and σ_1 as moderately NE (Fig. 2 inset) on the basis of the inferred thrust sense on the faults (Fig. 9c). The folds associated physically with these faults may be kinematically related since fold axes are also oriented parallel to the intersections between fault planes, suggesting that they share a similar intermediate stress axis, σ_2 (Fig. 2 inset).

7. Geochemistry

In order to understand the possible role of fluids and element mobility in mylonitization, we analysed the different kinds of mylonitic rocks formed after diatexites and compared them to potential protoliths, including weakly deformed migmatites and granites from the Tolombón complex. Whole-rock major element analyses (Table 1) were conducted on a Bruker-AXS S4 Pioneer X-ray Fluorescence Spectrometer at the Advanced Analytical Centre at

James Cook University, Queensland, Australia. Trace element analyses (Table 1) were conducted on the ICP-MS at Monash University, Victoria, Australia.

Major element and REE analyses of migmatites and granites from the Tolombón complex define a wide field whereas the mylonitic rocks plot in a narrower band within this field (Fig. 10). Major element analyses show that mylonitic rocks are enriched in SiO_2 and TiO_2 relative to the rocks of the Tolombón complex. REE analyses indicate a negative Eu anomaly and a negative REE slope. Mylonitic rocks show a relative LREE enrichment and HREE depletion with La/Lu ratios between 8.05 and 18.13 (Fig. 10b,d). The rocks of the Tolombón complex define a broad field with granites generally enriched in LREE, and migmatites enriched in HREE. For both major element and REE analyses there is no systematic variation within the mylonitic rocks on the basis of degree of mylonitization.

In Section 3.5 we described field observations of weakly deformed granitic diatexite (at point SQ183) transitioning into the layer of ultramylonitic diatexite. We plotted the major element (Fig. 10c) and REE (Fig. 10d) abundances of two weakly deformed but different samples of granitic diatexite from outcrop SQ183 (Fig. 2) and one sample of mylonitic metatexite from outcrop SQ194 with samples of the ultramylonitic diatexites. The two weakly deformed granitic diatexites and the mylonitic metatexite are geochemically almost identical to each other and differ slightly from samples of the ultramylonitic diatexites showing lower HREE and higher LREE.

Table 1
Major and rare earth element analyses of mylonitic rocks and their protoliths from the Tolombón complex.

Description	Ultramylonite						Mylonite				Protomylonite		Granite						
Sample	SQ187c	SQ80a	SQ29b	SQ37b	SQ77c	SQ79a	SQ187a	SQ187d	SQ29a	SQ77b	SQ77a	SQ30a	SQ133	SQ134	SQ130a	SQcndgr	SQ144	SQ131	SQ70c
Wt.% oxide																			
SiO ₂	67.20	71.99	69.48	67.72	69.55	69.09	67.56	67.19	69.07	69.83	68.95	69.47	74.10	72.47	71.90	68.58	65.99	71.52	73.33
TiO	0.74	0.72	0.74	0.95	0.69	0.72	0.73	0.69	0.73	0.66	0.76	0.77	0.04	0.23	0.23	0.64	0.60	0.23	0.36
Al ₂ O ₃	14.14	13.18	14.01	14.79	14.57	14.68	14.59	13.96	14.45	14.46	14.15	14.03	14.10	14.99	15.06	14.85	15.28	15.16	13.85
FeO	5.13	4.70	4.90	5.79	4.46	4.50	4.96	4.57	4.72	4.35	4.93	4.93	0.46	1.98	2.18	4.38	4.73	1.92	1.70
MnO	0.10	0.06	0.09	0.11	0.06	0.07	0.09	0.07	0.07	0.06	0.08	0.08	0.01	0.03	0.09	0.05	0.08	0.04	0.02
MgO	2.13	2.04	1.79	2.86	1.66	1.65	1.99	2.33	1.77	1.56	1.86	2.07	0.06	0.81	0.69	2.31	2.18	0.81	0.66
CaO	1.72	0.85	1.49	1.60	1.33	1.52	1.67	2.71	1.82	0.60	1.58	1.52	0.33	2.28	1.79	1.08	1.52	1.76	1.11
Na ₂ O	2.46	1.77	2.47	1.98	2.43	2.63	2.30	2.53	2.81	2.69	2.23	2.03	2.70	4.22	3.69	1.77	2.65	3.75	2.65
K ₂ O	4.09	2.71	3.53	3.53	3.56	3.69	3.60	3.27	3.40	3.63	3.50	3.53	6.72	1.40	3.53	4.44	4.31	3.57	5.50
P ₂ O ₅	0.11	0.13	0.20	0.08	0.23	0.21	0.09	0.31	0.19	0.24	0.23	0.17	0.12	0.14	0.17	0.29	0.29	0.20	0.13
Total	97.82	98.15	98.70	99.41	98.54	98.76	97.58	97.63	99.03	98.08	98.27	98.60	98.64	98.54	99.34	98.38	97.63	98.95	99.31
Chondrite normalised																			
Ce	161.95	139.62					165.67	116.10			140.27	117.90	37.70	111.76	60.82	104.99	109.11	72.26	
Pr	121.69	103.54					123.70	89.75			102.16	89.55	30.68	84.65	47.22	81.24	82.88	55.87	
Nd	93.44	78.12					94.33	70.10			77.80	68.38	23.49	64.57	36.25	64.33	63.63	42.18	
Sm	62.67	50.16					62.18	51.14			52.71	44.79	19.46	43.20	27.33	45.27	44.93	29.22	
Eu	22.16	22.67					23.04	22.14			21.57	19.78	9.57	14.97	13.51	25.88	19.32	13.66	
Gd	43.10	31.48					39.52	35.10			35.06	29.93	14.94	27.12	18.40	30.62	29.30	18.48	
Tb	41.51	27.10					33.08	30.58			32.02	26.64	16.47	23.52	18.24	29.27	26.25	16.69	
Dy	38.82	22.52					27.73	22.86			27.81	22.94	16.15	19.83	16.76	24.43	21.56	13.57	
Ho	39.91	20.94					25.51	17.64			26.14	21.97	16.39	18.33	16.51	19.31	18.96	11.64	
Er	36.73	18.98					20.73	13.02			23.60	19.92	15.10	16.40	16.01	12.40	16.16	9.81	
Tm	30.58	16.97					15.49	9.61			20.47	17.51	12.94	14.26	15.60	6.84	13.73	8.48	
Yb	27.39	16.24					12.89	8.59			19.38	16.43	11.65	13.71	16.18	4.65	12.75	8.03	
Lu	26.07	16.05					11.68	8.38			18.52	15.59	10.83	13.31	16.15	3.97	12.09	7.62	
Description																			
	Granitic diatexite						Stromatic metatexite					Melanosome				Leucosome			
Sample	SQ183	SQ183b	SQ132a	SQ120a	SQ114	SQ136c	SQ37a	SQ90c	SQ194a	SQ47a1	SQ50c	SQ65	SQ73a2	SQ136b	SQ70a	SQ132b			SQ50b
Wt.% oxide																			
SiO ₂	68.79	66.43	73.11	62.93	67.97	62.63	69.12	74.56	62.75	42.68	61.39	65.31	64.46	67.73	73.38	67.43			71.43
TiO	0.58	0.81	0.58	0.67	0.89	1.17	0.69	0.62	0.89	1.36	0.88	0.90	0.93	0.76	0.72	0.75			0.16
Al ₂ O ₃	13.84	13.83	12.36	17.45	14.58	16.55	13.80	10.43	16.37	28.44	17.30	15.99	16.80	14.74	12.60	15.51			16.53
FeO	5.34	5.77	4.33	6.40	4.94	8.61	4.15	3.81	8.08	11.65	8.86	6.42	5.17	6.78	4.20	6.35			2.31
MnO	0.11	0.06	0.12	0.16	0.07	0.08	0.06	0.08	0.15	0.17	0.14	0.07	0.05	0.07	0.04	0.10			0.03
MgO	2.29	2.65	1.52	2.52	2.23	2.52	1.99	1.56	2.82	5.59	3.10	3.05	2.69	2.43	2.06	2.61			0.61
CaO	2.41	1.38	0.92	1.54	1.96	2.08	2.32	1.24	0.97	0.50	0.77	1.58	1.49	1.57	1.66	1.22			0.68
Na ₂ O	2.35	1.81	1.96	2.30	3.46	2.46	2.43	2.13	2.21	0.79	1.58	2.32	3.08	2.17	2.17	2.13			2.02
K ₂ O	2.81	4.27	3.91	4.50	2.53	2.55	3.35	2.98	3.96	5.66	3.80	2.65	3.94	2.89	2.43	2.91			4.77
P ₂ O ₅	0.13	0.07	0.09	0.34	0.09	0.09	0.08	0.08	0.10	0.09	0.08	0.11	0.14	0.09	0.15	0.08			0.08
Total	98.65	97.08	98.89	98.81	98.73	98.73	97.99	97.49	98.30	96.93	97.90	98.39	98.74	99.22	99.40	99.08			98.62
Chondrite normalised																			
Ce	203.48	170.83	136.15	130.35	143.38	287.38	146.36	59.07	149.72		173.63	148.76	160.97	188.14	148.68				
Pr	154.40	127.12	100.90	96.62	103.72	207.88	109.91	43.70	108.66		119.68	113.21	117.78	141.79	109.24				
Nd	119.38	96.85	76.28	74.28	77.87	156.91	82.91	32.55	81.94		88.45	88.90	89.44	108.42	82.61				
Sm	73.51	57.61	49.33	53.36	49.43	93.58	53.97	22.52	52.21		53.62	57.17	55.25	71.11	52.09				
Eu	24.60	22.39	18.01	20.55	14.39	25.26	25.18	10.11	25.26		23.13	27.65	30.27	27.89	22.14				
Gd	44.28	33.66	32.36	40.41	30.75	55.47	33.25	17.89	34.48		33.38	35.54	34.63	44.05	32.36				
Tb	32.38	24.05	28.92	44.72	26.18	39.79	29.36	23.23	29.89		27.55	27.61	27.72	32.49	25.77				
Dy	23.04	17.20	26.30	46.69	20.91	26.28	26.53	29.64	22.94		22.37	19.24	20.91	21.00	18.79				
Ho	18.00	13.20	27.43	52.42	17.84	18.50	28.21	39.74	17.92		20.32	13.84	17.25	13.85	14.66				
Er	13.74	9.96	27.47	55.64	14.58	11.98	29.55	47.04	13.52		18.22	9.57	13.71	8.07	10.93				
Tm	10.76	7.77	27.03	55.10	11.17	7.42	28.27	49.74	10.39		16.15	6.71	10.71	4.47	8.05				
Yb	10.32	7.35	28.95	57.49	9.21	5.85	28.27	52.92	9.11		15.49	5.84	9.60	3.45	7.03				
Lu	10.31	7.34	29.40	59.56	8.14	5.36	27.13	55.72	8.59		15.36	5.62	9.39	3.10	6.66				

8. Discussion

Very few shear zones worldwide contain ultramylonites that are as thick as the PSZ. Here we discuss the geochemistry, shear strain, and tectonic setting of the PSZ to constrain the environment and understand the context in which thick ultramylonites develop.

8.1. Protolith of the mylonitic rocks

The nature of the protolith to the mylonitic rocks can be seen in transition zones between weakly deformed rocks and mylonitic rocks both for metatexites and diatexites. These transitions suggest that the Tolombón complex rocks are the protolith to the mylonitic

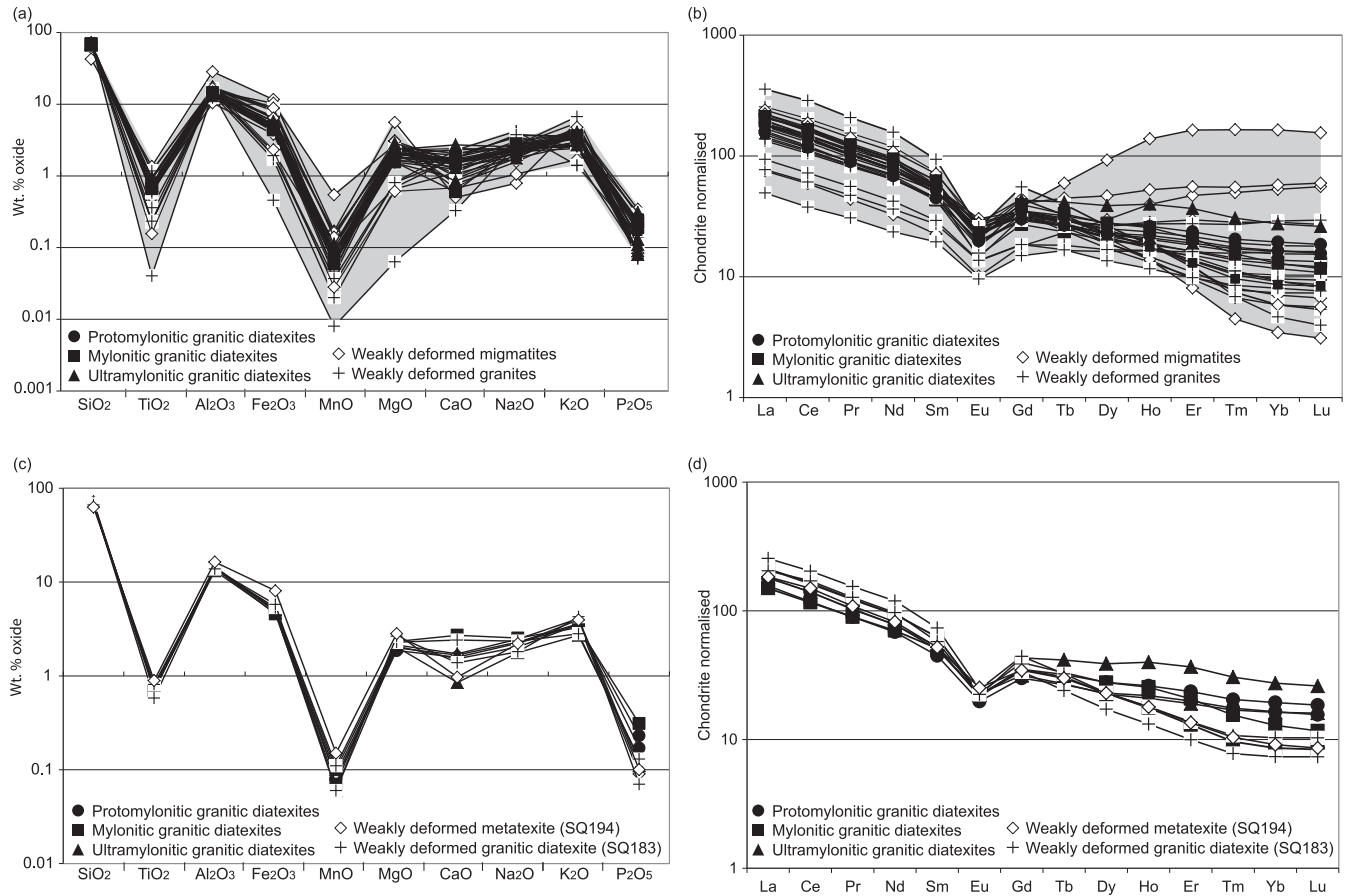


Fig. 10. (a) Major element and (b) chondrite-normalised (Sun and McDonough, 1989) REE abundances of weakly deformed migmatites and granites of the Tolombón complex (white symbols) and of the mylonitic rocks from the ultramylonitic diatexite layer of the El Pichao shear zone (black symbols). Spread of data of weakly deformed migmatites and granites defines a field (shaded in grey) which encompasses the narrower band defined by mylonitic rocks. (c) Major element and (d) chondrite-normalised REE abundances of migmatitic rocks that transition directly into mylonitic rocks.

rocks of the PSZ as further supported by the geochemistry. The fact that the mylonites show less compositional variation than the protoliths (Fig. 10) suggests the possibility of homogenization through shearing, which stretched and folded layering and caused mixing of phases through rotation of porphyroclasts (Fig. 8b,c,f). There is no systematic difference in geochemistry between protomylonites, mylonites, and ultramylonites. Taken together, this indicates that mylonitization was not accompanied by a progressive change in the chemistry of the rock, as has been identified in other shear zones (e.g. Oliot et al., 2010; Goncalves et al., 2012).

Structurally above the PSZ, strain decreases and the migmatites contain structures that indicate that melt was present during and facilitated folding and thrusting to the W, suggesting syn-kinematic anatexis (Fig. 4d,e; see Büttner et al., 2005; Weinberg and Mark, 2008; Weinberg et al., 2013). Deformation within the PSZ overprints and folds these early structures during amphibolite facies solid-state deformation that maintains broadly similar kinematics to the syn-anatectic deformation. This suggests that anatexis began during shearing and ceased with cooling as the rocks were thrust to higher structural levels. This cooling may have caused localization of thrusting to the PSZ where solid-state shearing continued.

8.2. Strain on the PSZ

From weakly deformed to mylonitic metatexites, there is a gradual strain increase described including an increase in the intensity of the foliation and the proportion of recrystallised matrix.

Strain increases further in the ultramylonitic diatexites, characterized by the nearly completely recrystallized matrix and naked clasts. Unlike mylonites, the foliation in ultramylonitic diatexites is poorly developed because mica-rich bands and quartz ribbons are absent. This is likely due to mixing and homogenization of the matrix facilitated by rolling feldspar clasts (Fig. 8a–c,f) and dissolution–precipitation of feldspars.

There is also a general decrease in grain size from protomylonitic to ultramylonitic rocks. Grain size is dependent, among other things, on temperature as well as stress, and it could be argued that the gradual decrease in grain size reflects a decrease in temperature and strain localization to zones of higher stresses. If this occurred, shearing in the PSZ would be at higher temperatures in the protomylonite and mylonite than in ultramylonite. While this is possible, the similarity in microstructures across the width of the shear zone indicates that shearing occurred at amphibolite facies in all rocks and so temperature variations were limited to between 500 and 700 °C. It is also possible that, independent of any temperature variations, stress distribution varied as a function of rock strength. As demonstrated by Regenauer-Lieb et al. (2006), it is possible that the system is controlled by neither constant strain rate nor constant stress (Platt and Behr, 2011) but by maximum energy dissipation. In this case weaker regions are zones of both high stress and high strain rate, and focus energy dissipation of the system. Thus, the decrease in grain size in ultramylonites would be a result of dynamic stress distribution.

The thickness of the ultramylonitic diatexite layer of the PSZ is estimated from its present-day dip and width across strike, disconsidering any possible post-shearing and mylonitization modifications caused by folding and faulting. The intra-mylonite folding is only minor and does not account for significant width modifications. Evidence for some post-mylonitization thickening is seen in the region of brittle overprint (Section 6) where pseudotachylites, breccias and brittle faults with a thrusting component may have caused some stacking of fault slivers. We are unable to ascertain if this brittle zone caused major repetition of fault slivers, however, our field evidence suggests relatively minor movements. If brittle faulting was a significant process and caused stacking of the shear zone, the continuous ultramylonitic layers on the footwall and hanging wall of the fault zone would still be hundreds of metres thick (Fig. 2).

Traditional methods to estimate strain in ductile shear zones use the angle between planes, deflection of markers, and changes in volume and shape of sheared objects (Ramsay and Graham, 1970; Ramsay, 1980). However, these structures are deformed to their maximum extent at shear strains lower than that required to form an ultramylonite because, for example, grains have been recycled several times (Norris and Cooper, 2003) and S planes are parallel to C planes at $\gamma \sim 29$ (using the method of Ramsay and Graham, 1970). Norris and Cooper (2003) estimated shear strain using the statistical change in thickness of pegmatite dykes. They found $\gamma > 120$ in mylonites and $\gamma > 180$ in ultramylonites, an order of magnitude higher than estimates using other methods (e.g. Mawer, 1983; Bailey et al., 1994; Wenk, 1998).

The PSZ ultramylonites show almost complete recrystallization of the matrix and homogenization of layering, destruction of quartz ribbons, and lack well-defined S–C fabric. Accordingly, there is no accurate way to estimate the total amount of movement. Given the current 40° dip of the shear zone, and the relatively small differences in metamorphic conditions between the hanging wall (granulite facies) and footwall (amphibolite facies), we postulate that the thrust had only a relatively small throw. This would imply either a small total movement, that the dip decreases at depth, or that the shear zone has steepened as a result of later (Andean?) crustal tilting.

8.3. Mylonitic shear zones of the Sierras Pampeanas

The Sierras Pampeanas include some very prominent shear zones such as the 16 km-thick Tres Arboles or Guachacorrall shear zone in the Sierras de Córdoba (Fig. 1; Whitmeyer and Simpson, 2003) and the 4 km-thick La Chilca shear zone (Larrovere et al., 2008). These shear zones trend N–S, thrust rocks to the west (Le Corre and Rossello, 1994; van Staal et al., 2011), and formed during the Pampean and Famatinian orogenies, between 535 and 450 Ma, with some dating to the Oclóyic tectonic phase between 450 and 430 Ma (Dalla Salda et al., 1992; Rapela et al., 1998a; Astini and Davila, 2004; Collo et al., 2008; Castro de Machuca et al., 2012). Similar to all major shear zones in the Sierras Pampeanas, the PSZ places higher grade rocks (Tolombón complex) on lower grade rocks (Agua del Sapo complex), which is compatible with thrusting, and contradicts the interpretation by Büttner (2009) that this is a tilted extensional terrane.

In Sierra de Quilmes, a terrane undergoing anatexis at 470 Ma, perhaps part of the Famatinian back-arc, was thrust to higher structural levels by generalised ductile shearing, such as recorded by syn-kinematic leucosomes in rocks north of the PSZ, near Laguna (Fig. 1b). These rocks cooled, anatexis ceased, and strain localized into the 3.5 km-wide PSZ. Localization of strain to the PSZ may have caused cessation of shearing north of the PSZ preserving high-temperature magmatic structures. In the PSZ

shearing continued at amphibolite facies producing the ultramylonites and mylonites which obliterated the pre-existing high-temperature structures. Localization during cooling has also been inferred for the Arenosa Creek shear zone in the western Sierras Pampeanas where shearing began at granulite facies conditions (>800 °C) and continued to temperatures of 500–700 °C (Castro de Machuca et al., 2012). This is also similar to the Tres Arboles shear zone (Fig. 1a) which underwent migmatization during the Pampean Orogeny and records deformation temperatures between 540 and 590 °C and pressures of 3–6 kbar (Whitmeyer and Simpson, 2003). Other shear zones of the Sierras Pampeanas show greenschist–amphibolite facies shearing with no evidence of an early higher temperature event. For example, the El Tigre shear zone (Fig. 1a) deformed at temperatures of 300–400 °C (Fig. 1a; Castro de Machuca et al., 2010), the Las Pirquitas thrust formed at amphibolite facies (Fig. 1a; van Staal et al., 2011) and La Chilca shear zone (Fig. 1a) deformed at temperatures of 350–500 °C but also overprints migmatites (Larrovere et al., 2008).

The brittle overprint mapped within the PSZ has also been recorded in other mylonitic shear zones of the Sierras Pampeanas (e.g. Whitmeyer and Simpson, 2003; Delpino et al., 2007). The Sierras Pampeanas have a long history of tectonic activity and such low-temperature deformation could be related to tectonic events in the Mesozoic or Cenozoic (e.g. Delpino et al., 2007).

The length, breadth, and strain documented in the Sierras Pampeanas makes these shear zones of the Pampean and Famatinian orogenies comparable to major shear zones worldwide such as the shear zones of the Pan-African orogeny (Ferkous and Leblanc, 1995; Arthaud et al., 2008), the Mulgandinnah shear zone of the accreted Pilbara terrane in Australia (Zegers et al., 1998), and the Variscan Corredoiras detachment in NW Spain (Díaz García et al., 1999).

8.4. Processes that form thick ultramylonites

Thick ultramylonites are rare and whilst we have a reasonable understanding of the processes that form them (e.g. Poirier, 1980; White et al., 1980; Means, 1995; Kilian et al., 2011; Platt and Behr, 2011; Vauchez et al., 2012), we do not have a good understanding of what controls their final width. Shear zone width is dependent on strain rate, the total amount of strain, and the strength and strength evolution of the shear zone and surrounding rocks during deformation. At upper amphibolite to granulite facies, rock strength is low and strain is distributed producing a thick, low-strain shear zone (Vauchez et al., 2012). At lower temperatures, rock strength increases, which promotes strain localisation enabling formation of thin bands of ultramylonite. However, such variations cannot explain the existence of thick packages of ultramylonites. It has been suggested that the formation of thick shear zones requires shear zone widening which can occur when the rock on the margin of the shear zone becomes easier to deform than the shear zone interior (Means, 1995). This can be due to microstructural changes in the shear zone leading to strain-hardening or changes in the host rock which make it softer and easier to deform (Means, 1984; Hull, 1988; Mitra, 1992; Ingles et al., 1999; Rutter, 1999). Strain-hardening can occur through the accumulation of dislocations and changes in the style or mechanism of deformation (Passchier and Trouw, 2005; Johnson et al., 2011) or reaction-hardening through the growth of new minerals (Groome et al., 2006). The rock is strengthened and more difficult to deform due to the destruction of mica-rich shear planes or an increase in the proportion of dislocation tangles (Passchier and Trouw, 2005). Reaction induced softening can occur in the shear zone or in the host rock and is caused by the growth of new, softer minerals (White and Knipe, 1978; Hippert and Hongn, 1998).

The thick shear zones formed during the Pampean–Famatinian orogenies suggest that only a few major shear zones accommodated most of the crustal shortening driven by plate convergence. In the absence of significant rheological layering capable of controlling strain localization, the width of a shear zone may be determined by the balance between shear heat generation and diffusion. Small initial perturbations in shear heating localize the initial shear zone, which grows in width as a result of heat diffusion into colder surroundings. A quasi-static state can be reached, where the width of the shear zone (w) is:

$$w \sim \sqrt{\kappa/\dot{\epsilon}} \quad (1)$$

where $\dot{\epsilon}$ is the strain rate and the κ is thermal diffusivity (Regenauer-Lieb and Yuen, 2004). For $\kappa = 10^{-6} \text{ m}^2 \text{ s}^{-1}$ and strain rate between 10^{-14} s^{-1} and 10^{-12} s^{-1} , equation (1) yields a shear zone between 10 and 1 km thick, bracketing the 3.5 km width of the PSZ. If we assume that the 1 km-thick ultramylonitic section took up most of the strain across the shear zone, and impose a velocity of 30 mm/yr across that part of the shear zone, implying that it accommodates a significant proportion of characteristic plate convergence velocities, the strain rate across the ultramylonite would be 10^{-12} s^{-1} . For these values, a steady-state width balancing heat generation and diffusion would have been reached in only $\sim 0.03 \text{ Ma}$ ($t \sim w^2/\kappa$). Thus, we postulate that the dominance of very wide shear zones across the Pampean–Famatinian orogens of NW Argentina is a result of localization of strain into few dominant shear zones whose widths are controlled by the balance between shear heating and thermal diffusion.

9. Conclusions

The El Pichao shear zone is a $>3.5 \text{ km}$ thick shear zone that thrusts the granulitic migmatites of the Tolombón complex on the amphibolite facies rocks of the Agua del Sapo complex. At its base the shear zone comprises a $\sim 1 \text{ km}$ -thick ultramylonitic diatexite with a very fine, intensely recrystallized groundmass, a weak foliation, and naked clasts, generally from disrupted pegmatites. Strain decreases gradually to the NE until weakly deformed metatexites, diatexites, and granites crop out. Geochemistry indicates that the composition of the mylonitic rocks is similar to that of migmatites and granites, but less varied. We interpret this to indicate that the mylonitic rocks have been homogenized by stretching and folding but in an essentially closed system with negligible fluid and element mobility.

The Sierras Pampeanas is a high strain zone that has a discontinuous extent of over 1000 km and a width of 250 km (Larrovere et al., 2011) with a network of wide shear zones comparable in length and breadth to those of major orogens worldwide. Thick bands of mylonites and ultramylonites of the Sierras Pampeanas have accommodated top-to-west thrusting during the Pampean and Famatinian orogenies. In the PSZ anatexis was contemporaneous with the early stages of thrusting and preceded localization into the shear zone, which continued to deform in amphibolite facies eventually thrusting migmatites onto lower grade rocks. The shear zone was later reactivated and overprinted during brittle faulting at greenschist facies.

Thick ultramylonites such as those in the PSZ, although rare, bring up questions regarding the controls on the width of shear zones and strain distribution in an orogeny, together with questions regarding the distribution of stress and strain rate across a deforming mountain belt, and the nature and extent of strain localization. We speculate that in the absence of significant rheological heterogeneities, shear heating localizes crustal strain to a few wide shear zones capable of taking up a large proportion of plate

convergence velocity and forming thick mylonite–ultramylonite belts, as is common in the Pampean–Famatinian orogens.

Acknowledgements

We thank L. Wolfram for help with sample preparation and N. Hunter for assistance with grain size estimates. We also thank F. Hongn and A. Vauchez for their detailed and valuable reviews that helped us improve this manuscript. This work was financially supported by the Australian Research Council DP110102543. P. Hasalová acknowledges funding from the Czech National Grant Agency (grant 14-25995S).

References

- Acenolaza, F.G., Miller, H., Toselli, A.J., 1988. The Puncovicana Formation (Late Precambrian–Early Cambrian) – sedimentology, tectonometamorphic history and age of the oldest rocks of NW Argentina. In: Bahlburg, H., Breitkreuz, C., Giese, P. (Eds.), *The Southern Central Andes, Lecture Notes in Earth Sciences*, vol. 17. Springer-Verlag, Berlin.
- Arthaud, M.H., Caby, R., Fuck, R.A., Dantas, E.L., Parente, C.V., 2008. Geology of the northern Borborema Province, NE Brazil and its correlation with Nigeria, NW Africa. In: Pankhurst, R., Trouw, R.A.J., Brito Neves, B.B., de Wit, M.J. (Eds.), *West Gondwana: Pre-Cenozoic Correlations across the South Atlantic Region*, vol. 294. Geological Society of London, pp. 49–67.
- Astini, R.A., Davila, F.M., 2004. Ordovician back arc foreland and Oclóyic thrust belt development on the western Gondwana margin as a response to Precordillera terrane accretion. *Tectonics* 23, TC4008.
- Bahlburg, H., Herve, F., 1997. Geodynamic evolution and tectonostratigraphic terranes of northwestern Argentina and northern Chile. *GSA Bull.* 109 (7), 869–884.
- Bailey, C.M., Simpson, C., De Paor, D.G., 1994. Volume loss and tectonic flattening strain in granitic mylonites from the Blue Ridge province, central Appalachians. *J. Struct. Geol.* 16 (10), 1403–1416.
- Becchio, R., Lucassen, F., Kasemann, S.F., Franz, G., Viramonte, J., 1999. Geoquímica y sistemática isotópica de rocas metamórficas del Paleozoico inferior: Noroeste de Argentina y Norte de Chile (21°–27°S). *Acta Geol. Hisp.* 34, 273–299.
- Büttner, S.H., 2009. The Ordovician Sierras Pampeanas–Puna basin connection: basement thinning and basin formation in the Proto-Andean back-arc. *Tectonophysics* 477 (3–4), 278–291.
- Büttner, S.H., Glodny, J., Lucassen, F., Wemmer, K., Erdmann, S., Handler, R., Franz, G., 2005. Ordovician metamorphism and plutonism in the Sierra de Quilmes metamorphic complex: implications for the tectonic setting of the northern Sierras Pampeanas (NW Argentina). *Lithos* 83 (1–2), 143–181.
- Castro de Machuca, B., Delpino, S., Previley, L., Mogessie, A., Bjerg, E., 2012. Tectonometamorphic evolution of a high- to medium-grade ductile deformed meta-gabbro/metadiorite from the Arenosa Creek Shear Zone, Western Sierras Pampeanas, Argentina. *J. Struct. Geol.* 42, 261–278.
- Castro de Machuca, B., Morata, D., Pontoriero, S., Arancibia, G., 2010. Textural variations and chemical mobility during mylonitization: the El Tigre granitoid shear zone, Sierra de Pie de Palo, Western Sierras Pampeanas, San Juan. *Rev. Asoc. Geol. Argent.* 66 (1), 54–65.
- Collo, G., Astini, R.A., Cardona, A., Do Campo, M.D., Cordani, U., 2008. Metamorphic ages of low-grade units in the central region of Famatina: the signature of the Oclóyic Orogeny (Ordovician). *Rev. Geol. Chile* 35 (2), 191–213.
- Dalla Salda, L.H., Cingolani, C.A., Varela, R., 1992. Early Paleozoic orogenic belt of the Andes in southwestern South America: result of Laurentia–Gondwana collision? *Geology* 20, 617–620.
- Delpino, S.H., Bjerg, E.A., Ferracutti, G.R., Mogessie, A., 2007. Counterclockwise tectonometamorphic evolution of the Pringles metamorphic complex, Sierras Pampeanas of San Luis (Argentina). *J. South Am. Earth Sci.* 23 (2–3), 147–175.
- Díaz García, F., Martínez Catalán, J.R., Arenas, R., González Cuadra, P., 1999. Structural and kinematic analysis of the Carredoiras detachment: evidence for early Variscan synconvergent extension in the Ordenes Complex, NW Spain. *Int. J. Earth Sci.* 88, 337–351.
- Ferkous, K., Leblanc, M., 1995. Gold mineralisation in the West Hoggar shear zone, Algeria. *Miner. Deposita* 30, 211–224.
- Fliervoet, T.F., White, S.H., Drury, M.R., 1997. Evidence for dominant grain-boundary sliding deformation in greenschist – and amphibolite-grade polymetamorphic ultramylonites from the Redbank deformed Zone, Central Australia. *J. Struct. Geol.* 19 (12), 1495–1520.
- Garlick, S.R., Gromet, L.P., 2004. Diffusion creep and partial melting in high temperature mylonitic gneisses, Hope Valley shear zone, New England Appalachians, USA. *J. Metamorph. Geol.* 22, 45–62.
- Goncalves, P., Olliot, E., Marquer, D., Connolly, J.A.D., 2012. Role of chemical processes on shear zone formation: an example from the Grimsel metagranodiorite (Aar massif, Central Alps). *J. Metamorph. Geol.* 30 (7), 703–722.
- Griera, A., Bons, P.D., Jessell, M.W., Lebensohn, R.A., Evans, L., Gomez-Rivas, E., 2011. Strain localisation and porphyroclast rotation. *Geology* 39 (3), 275–278.

- Groome, W.G., Johnson, S.E., Koons, P.O., 2006. The effects of porphyroblast growth on the effective viscosity of metapelitic rocks: implications for the strength of the middle crust. *J. Metamorph. Geol.* 24 (5), 389–407.
- Hanmer, S., Williams, M., Kopf, C., 1995. Modest movements, spectacular fabrics in an intracontinental deep-crustal strike-slip fault: striding-Athabasca mylonite zone, NW Canadian Shield. *J. Struct. Geol.* 17 (4), 493–507.
- Hippert, J.F., 1998. Breakdown of feldspar, volume gain and lateral mass transfer during mylonitization of granitoid in a low metamorphic grade shear zone. *J. Struct. Geol.* 20 (2–3), 175–193.
- Hippert, J.F., Hongn, F.D., 1998. Deformation mechanisms in the mylonite/ultramylonite transition. *J. Struct. Geol.* 20 (11), 1435–1448.
- Hirth, G., Tullis, J., 1992. Dislocation creep regimes in quartz aggregates. *J. Struct. Geol.* 14 (2), 145–159.
- Höckenreiner, M., Söllner, F., Miller, H., 2003. Dating the TIPA shear zone: an Early Devonian terrane boundary between the Famatinian and Pampean systems (NW Argentina). *J. South Am. Earth Sci.* 16 (1), 45–66.
- Hongn, F., Becchio, R., 1999. Las fajas miloníticas de Brealito, basamento del Valle Calchaqui, Salta, Argentina. *Rev. Asoc. Geol. Argent.* 54, 74–87.
- Hongn, F.D., Mon, R., Cuevas, J., Tubia, J.M., 1996. Zonas de cisaillement calédoniennes à haute température dans la quebrada Barranquilla (Puna Oriental, Argentina): données structurales et cinématiques. *Comp. Rend. Acad. Sci. Paris, Ila* 323, 809–815.
- Hongn, F.D., Riller, U., 2007. Tectonic evolution of the western margin of Gondwana inferred from syntectonic emplacement of Paleozoic granitoid plutons in Northwest Argentina. *J. Geol.* 115 (2), 163–180.
- Hongn, F.D., Tubia, J.M., Aranguren, A., Vegas, N., Mon, R., Dunning, G.R., 2010. Magmatism coeval with lower Paleozoic shelf basins in NW-Argentina (Tastil batholith): constraints on current stratigraphic and tectonic interpretations. *J. South Am. Earth Sci.* 29 (2), 289–305.
- Hull, J., 1988. Thickness–displacement relationships for deformation zones. *J. Struct. Geol.* 10 (4), 431–435.
- Ingles, J., Lamouroux, C., Soula, J.-C., Guerrero, N., Debat, P., 1999. Nucleation of ductile shear zones in a granulodite under greenschist facies conditions, Neuvillie massif, Pyrenees, France. *J. Struct. Geol.* 21 (5), 555–576.
- Ishii, K., Kanagawa, K., Shigematsu, N., Okudaira, T., 2007. High ductility of K-feldspar and development of granitic banded ultramylonite in the Ryoke metamorphic belt, SW Japan. *J. Struct. Geol.* 29 (6), 1083–1098.
- Jefferies, S.P., Holdsworth, R.E., Wibberley, C.A.J., Shimamoto, T., Spiers, C.J., Niemeijer, A.R., Lloyd, G.E., 2006. The nature and importance of phyllonite development in crustal-scale fault cores: an example from the Median Tectonic Line, Japan. *J. Struct. Geol.* 28 (2), 220–235.
- Jessell, M.W., Siebert, E., Bons, P.D., Evans, L., Piazzolo, S., 2005. A new type of numerical experiment on the spatial and temporal patterns of localization of deformation in a material with a coupling of grain size and rheology. *Earth Planet. Sci. Lett.* 239, 309–326.
- Jezeq, P., Willner, A.P., Acenolaza, F.G., Miller, H., 1985. The Puncoviscana trough – a large basin of Late Precambrian to Early Cambrian age on the Pacific edge of the Brazilian shield. *Geol. Rundsch.* 74 (3), 573–584.
- Ji, S., Jiang, Z., Rybacki, E., Wirth, R., Prior, D., Xia, B., 2004. Strain softening and microstructural evolution of anorthite aggregates and quartz–anorthite layered composites deformed in torsion. *Earth Planet. Sci. Lett.* 222 (2), 377–390.
- Johnson, S.E., Jin, Z.-H., Naus-Thijssen, F.M.J., Koons, P.O., 2011. Coupled deformation and metamorphism in the roof of a tabular midcrustal igneous complex. *GSA Bull.* 123 (5–6), 1016–1032.
- Jordan, T.E., Allmendinger, R.W., 1986. The Sierras Pampeanas of Argentina: a modern analogue of Rocky Mountain foreland deformation. *Am. J. Sci.* 286 (10), 737–764.
- Kanagawa, K., Shimano, H., Hiroi, Y., 2008. Mylonitic deformation of gabbro in the lower crust: a case study from the Pankenushi gabbro in the Hidaka metamorphic belt of central Hokkaido, Japan. *J. Struct. Geol.* 30 (9), 1150–1166.
- Kilian, R., Heilbronner, R., Stunitz, H., 2011. Quartz grain size reduction in a granitoid rock and the transition from dislocation to diffusion creep. *J. Struct. Geol.* 33 (8), 1265–1284.
- Larrovere, M.A., de los Hoyos, C.R., Toselli, A.J., Rossi, J.N., Basei, M.A.S., Belmar, M.E., 2011. High T/P evolution and metamorphic ages of the migmatitic basement of northern Sierras Pampeanas, Argentina: characterization of a mid-crustal segment of the Famatinian belt. *J. South Am. Earth Sci.* 31 (2–3), 279–297.
- Larrovere, M.A., Toselli, A.J., Rossi De Toselli, J.N., 2008. Petrología y estructura de la Faja de deformación La Chilca, Catamarca. *Rev. Asoc. Geol. Argent.* 63 (2), 254–263.
- Le Corre, C.A., Rossello, E.A., 1994. Kinematics of Early Paleozoic ductile deformation in the basement of NW Argentina. *J. South Am. Earth Sci.* 7 (3–4), 301–308.
- Loewy, S.L., Connolly, J.N., Dalziel, I.W.D., 2004. An orphaned basement block: the Arequipa–Antofalla Basement of the central Andean margin of South America. *GSA Bull.* 116 (1–2), 171–187.
- Lopez, J.P., Grosse, P., Toselli, A., 2007. Faja de deformación La Horqueta, Sierra de Velasco, Sierras Pampeanas, NO de Argentina: petrografía, geoquímica, estructuras y significado tectónico. *Estud. Geol.* 63 (2), 5–18.
- Lopez, J.P., Toselli, A.J., 1993. La faja milonítica TIPA: Faldeo oriental del Sistema de Famatina. In: XII Congreso Geológico Argentino y II Congreso de Exploración de Hidrocarburos III, Mendoza, pp. 39–42.
- Lucassen, F., Becchio, R., 2003. Timing of high-grade metamorphism: Early Palaeozoic U–Pb formation ages of titanite indicate long-standing high-T conditions at the western margin of Gondwana (Argentina, 26–29°S). *J. Metamorph. Geol.* 21 (7), 649–662.
- Lucassen, F., Becchio, R., Franz, G., 2011. The Early Palaeozoic high-grade metamorphism at the active continental margin of West Gondwana in the Andes (NW Argentina/N Chile). *Int. J. Earth Sci.* 100 (2), 445–463.
- Lucassen, F., Becchio, R., Wilke, H.G., Franz, G., Thirlwall, M.F., Viramonte, J., Wemmer, K., 2000. Proterozoic–Paleozoic development of the basement of the Central Andes (18–26°S) – a mobile belt of the South American craton. *J. South Am. Earth Sci.* 13, 697–715.
- Martino, R.D., 2003. Las fajas de deformación ductil de las Sierras Pampeanas de Córdoba: Una reseña general. *Rev. Asoc. Geol. Argent.* 58 (4), 549–571.
- Mawer, C.K., 1983. State of strain in a quartzite mylonite, Central Australia. *J. Struct. Geol.* 5, 401–409.
- Means, W.D., 1984. Shear zones of types I and II and their significance for reconstruction of rock history. *Geol. Soc. Am. Abstr. Programs* 16, 50.
- Means, W.D., 1995. Shear zones and rock history. *Tectonophysics* 247 (1–4), 157–160.
- Mehnert, K.R., 1968. Migmatites and the Origin of Granitic Rocks. Elsevier, Amsterdam, Netherlands.
- Mitra, G., 1992. Deformation of granitic basement rocks along fault zones at shallow to intermediate crustal levels. In: Mitra, S., Fisher, G.W. (Eds.), *Structural Geology of Fold and Thrust Belts*. Johns Hopkins University Press, Baltimore, MD, pp. 123–144.
- Montési, L.G.J., Zuber, M.T., 2002. A unified description of localization for application to large-scale tectonics. *J. Geophys. Res.* 107 (B3), 1–21.
- Norris, R.J., Cooper, A.F., 2003. Very high strains recorded in mylonites along the Alpine Fault, New Zealand: implications for the deep structure of plate boundary faults. *J. Struct. Geol.* 25 (12), 2141–2157.
- O'Hara, K., 2007. Reaction weakening and emplacement of crystalline thrusts: diffusion control on reaction rate and strain rate. *J. Struct. Geol.* 29 (8), 1301–1314.
- Oliot, E., Goncalves, P., Marquer, D., 2010. Role of plagioclase and reaction softening in a metagranite shear zone at mid-crustal conditions (Gotthard Massif, Swiss Central Alps). *J. Metamorph. Geol.* 28 (8), 849–871.
- Omarini, R.H., Sureda, R.J., Gotze, H.-J., Seilacher, A., Pfluger, F., 1999. Puncoviscana folded belt in northwestern Argentina: testimony of Late Proterozoic Rodinia fragmentation and pre-Gondwana collisional episodes. *Int. J. Earth Sci.* 88, 76–97.
- Passchier, C.W., Trouw, R.A.J., 2005. *Microtectonics*. Springer-Verlag, Berlin, Heidelberg.
- Pennacchioni, G., Mancktelow, N.S., 2007. Nucleation and initial growth of a shear zone network within compositionally and structurally heterogeneous granulites under amphibolite facies conditions. *J. Struct. Geol.* 29 (11), 1757–1780.
- Platt, J.P., Behr, W.M., 2011. Lithospheric shear zones as constant stress experiments. *Geology* 39 (2), 127–130.
- Poirier, J.P., 1980. Shear localization and shear instability in materials in the ductile field. *J. Struct. Geol.* 2 (1–2), 135–142.
- Ramos, V.A., 1988. Late-Proterozoic–Early Paleozoic of South America: a collisional history. *Episodes* 11, 168–175.
- Ramsay, J.G., 1980. Shear zone geometry: a review. *J. Struct. Geol.* 2 (1/2), 83–99.
- Ramsay, J.G., Graham, R.H., 1970. Strain variation in shear belts. *Can. J. Earth Sci.* 7, 786–813.
- Rapela, C., 1976. El basamento metamórfico de la región de Cafayate, Provincia de Salta. Aspectos petrológicos y geoquímicos. *Rev. Asoc. Geol. Argent.* 31, 203–222.
- Rapela, C.W., Pankhurst, R.J., Casquet, C., Baldo, E., Saavedra, J., Galindo, C., 1998a. Early evolution of the Proto-Andean margin of South America. *Geology* 26 (8), 707–710.
- Rapela, C.W., Pankhurst, R.J., Casquet, C., Baldo, E., Saavedra, J., Galindo, C., Fanning, C.M., 1998b. The Pampean Orogeny of the southern proto-Andes: Cambrian continental collision in the Sierras de Córdoba. *Geol. Soc. Lond. Spec. Publ.* 142 (1), 181–217.
- Regenauer-Lieb, K., Weinberg, R.F., Rosenbaum, G., 2006. The effect of energy feedbacks on continental strength. *Nature* 442 (7098), 67–70.
- Regenauer-Lieb, K., Weinberg, R.F., Rosenbaum, G., 2012. The role of elastic stored energy in controlling the long term rheological behaviour of the lithosphere. *J. Geodyn.* 55, 66–75.
- Regenauer-Lieb, K., Yuen, D.A., 1998. Rapid conversion of elastic energy into plastic shear heating during incipient necking of the lithosphere. *Geophys. Res. Lett.* 25 (14), 2737–2740.
- Regenauer-Lieb, K., Yuen, D.A., 2004. Positive feedback of interacting ductile faults from coupling of equation of state, rheology and thermal-mechanics. *Phys. Earth Planet. Interiors* 142, 113–135.
- Rossi De Toselli, J.N., Toselli, A., Toselli, G., 1976. Migmatización y metamorfismo en el basamento de la Sierra de Quilmes, al oeste de Colalao del Valle, Provincia de Tucumán, Argentina. *Rev. Asoc. Geol. Argent.* 31 (2), 83–94.
- Rutter, E.H., 1999. On the relationship between the formation of shear zones and the form of the flow law for rocks undergoing dynamic recrystallization. *Tectonophysics* 303 (1–4), 147–158.
- Sawyer, E.W., 2008. *Atlas of Migmatites*. NRC Research Press, Ottawa, Ontario, Canada.
- Schwartz, J.J., Gromet, L.P., 2004. Provenance of a late Proterozoic–early Cambrian basin, Sierras de Córdoba, Argentina. *Precambrian Res.* 129, 1–21.
- Sibson, R.H., 1977. Fault rocks and fault mechanisms. *J. Geol. Soc. Lond.* 133, 191–213.

- Sims, J.P., Ireland, T.R., Camacho, A., Lyons, P., Pieters, P.E., Skirrow, R.G., Stuart-Smith, P.G., Miro, R., 1998. U–Pb, Th–Pb and Ar–Ar geochronology from the southern Sierras Pampeanas, Argentina: implications for the Palaeozoic tectonic evolution of the western Gondwana margin. *Geol. Soc. Lond. Spec. Publ.* 142 (1), 259–281.
- Sinha, A.K., Hewitt, D.A., Rimstidt, J.D., 1986. Fluid interaction and element mobility in the development of ultramylonites. *Geology* 14, 883–886.
- Sola, A.M., Becchio, R.A., Pimentel, M., 2010. Leucogranito Pumayaco: anatexis cortical durante el ciclo orogenico Famatiniano en el extremo norte de la Sierra del Molinos, Provincia de Salta. *Rev. Asoc. Geol. Argent.* 66 (1), 206–224.
- Stunitz, H., Gerald, J.D.F., 1993. Deformation of granitoids at low metamorphic grade. II: granular flow in albite-rich mylonites. *Tectonophysics* 221 (3–4), 299–324.
- Sun, S.-s., McDonough, W.F., 1989. Chemical and isotopic systematics of oceanic basalts: implication for mantle composition and processes. In: Saunders, A.D., Norry, M.J. (Eds.), *Magmatism in Ocean Basins*, vol. 42. Geological Society London Special Publication, pp. 313–345.
- Toselli, A., Rossi De Toselli, J.N., Rapela, C.W., 1978. El basamento metamorfoico de la Sierra de Quilmes, Republica Argentina. *Rev. Asoc. Geol. Argent. Rev.* 33 (2), 105–121.
- Trouw, R.A.J., Passchier, C.W., Wiersma, D.J., 2010. *Atlas of Mylonites – and Related Structures*. Springer, Berlin, Heidelberg.
- Tullis, J., Snoke, A.W., Todd, V.R., 1982. Significance and petrogenesis of mylonitic rocks. *Geology* 10, 227–230.
- Tullis, J., Yund, R.A., 1985. Dynamic recrystallization of feldspar: a mechanism for ductile shear zone formation. *Geology* 13 (4), 238–241.
- Turner, J.C., 1960. Estratigrafia de la Sierra de Santa Victoria y adyacencias. *Boletin Acad. Nac. Ciencias, Cordoba* 41 (2), 163–206.
- van Staal, C.R., Vujovich, G.I., Currie, K.L., Naipauer, M., 2011. An Alpine-style Ordovician collision complex in the Sierra de Pie de Palo, Argentina: record of subduction of Cuyania beneath the Famatina arc. *J. Struct. Geol.* 33 (3), 343–361.
- Vauchez, A., Egydio-Silva, M., Babinski, M., Tommasi, A., Uhlein, A., Liu, D., 2007. Deformation of a pervasively molten middle crust: insights from the neo-proterozoic Ribeira-Araçuaí orogen (SE Brazil). *Terra Nova* 19 (4), 278–286.
- Vauchez, A., Tommasi, A., 2003. Wrench faults down to the asthenosphere: geological and geophysical evidence and thermomechanical effects. *Geol. Soc. Lond. Spec. Publ.* 210 (1), 15–34.
- Vauchez, A., Tommasi, A., Mainprice, D., 2012. Faults (shear zones) in the Earth's mantle. *Tectonophysics* 558–559, 1–27.
- Waters, D.J., 2001. The significance of prograde and retrograde quartz-bearing intergrowth microstructures in partially melted granulite-facies rocks. *Lithos* 56 (1), 97–110.
- Weinberg, R.F., Hasalova, P., Ward, L., Fanning, C.M., 2013. Interaction between deformation and magma extraction in migmatites: examples from Kangaroo Island, South Australia. *GSA Bull.* 125 (7–8), 1282–1300.
- Weinberg, R.F., Mark, G., 2008. Magma migration, folding and disaggregation of migmatites in the Karakoram shear zone, Ladakh, NW India. *GSA Bull.* 120, 994–1009.
- Wenk, H.-R., 1998. Deformation of mylonites in Palm Canyon, California, based on xenolith geometry. *J. Struct. Geol.* 20 (5), 559–571.
- White, S.H., Burrows, S.E., Carreras, J., Shaw, N.D., Humphreys, F.J., 1980. On mylonites in ductile shear zones. *J. Struct. Geol.* 2 (1–2), 175–187.
- White, S.H., Knipe, R.J., 1978. Transformation- and reaction-enhanced ductility in rocks. *J. Geol. Soc. Lond.* 135 (5), 513–516.
- Whitmeyer, S.J., Simpson, C., 2003. High strain-rate deformation fabrics characterize a kilometers-thick Paleozoic fault zone in the Eastern Sierras Pampeanas, central Argentina. *J. Struct. Geol.* 25 (6), 909–922.
- Whitney, D.L., Evans, B.W., 2010. Abbreviations for names of rock-forming minerals. *Am. Mineral.* 95, 185–187.
- Zegers, T.E., de Keijzer, M., Passchier, C.W., White, S.H., 1998. The Mulgandinnah shear zone; an Archean crustal scale strike-slip zone, eastern Pilbara, Western Australia. *Precambrian Res.* 88, 233–247.